Article

Cell

KPC1-Mediated Ubiquitination and Proteasomal Processing of NF-κB1 p105 to p50 Restricts Tumor Growth

Graphical Abstract

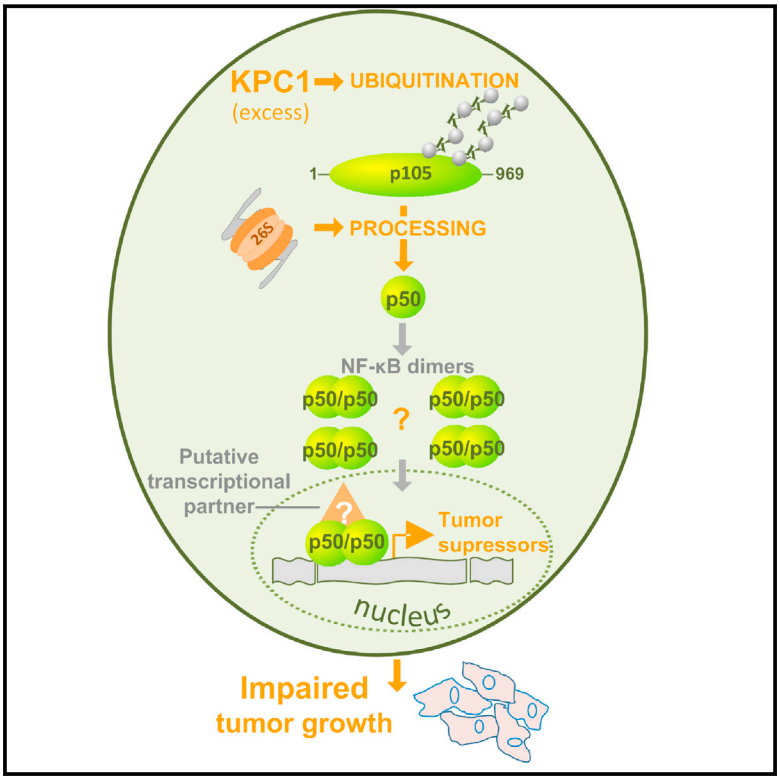

Highlights

- KPC1 ubiquitinates p105, resulting in its basal and signal-induced cleavage to p50
- KPC1 inhibits tumor growth via regulation of p50-dependent tumor suppressor genes
- KPC1 and p50 levels are correlated and are lower in tumors than in normal tissue
- Excess p50 downregulates p65, possibly lowering tumorigenic levels of p50-p65 NF-κB

Authors

Yelena Kravtsova-Ivantsiv, Inna Shomer, ..., Ilana Doweck, Aaron Ciechanover

Correspondence

aaroncie@tx.technion.ac.il

In Brief

KPC1-dependent ubiquitination of p105 supports limited processing to produce p50, thereby shaping the population of NF-κB subunits available. Production of p50 appears linked to a tumor-suppressive expression pattern and suggests a balancing of NF-κB's roles in tumorigenesis.

Accession Numbers

GSE60530

Kravtsova-Ivantsiv et al., 2015, Cell *161*, 333–347
April 9, 2015
http://dx.doi.org/10.1016/j.cell.2015.03.001

CellPress

Cell

KPC1-Mediated Ubiquitination and Proteasomal Processing of NF-κB1 p105 to p50 Restricts Tumor Growth

Yelena Kravtsova-Ivantsiv,[1,13] Inna Shomer,[1,13] Victoria Cohen-Kaplan,[1] Berend Snijder,[2] Giulio Superti-Furga,[2] Hedva Gonen,[1] Thomas Sommer,[3] Tamar Ziv,[4] Arie Admon,[4] Inna Naroditsky,[5] Muhammad Jbara,[6] Ashraf Brik,[6,7] Eli Pikarsky,[8,9] Yong Tae Kwon,[10,11] Ilana Doweck,[12] and Aaron Ciechanover[1,10,11,*]

[1]The David and Janet Polak Cancer and Vascular Biology Research Center, The Rappaport Faculty of Medicine and Research Institute, Technion-Israel Institute of Technology, Haifa 31096, Israel

[2]CeMM Research Center for Molecular Medicine of the Austrian Academy of Sciences, Vienna 1090, Austria

[3]Max Delbrück Center for Molecular Medicine, Berlin 13125, Germany

[4]The Smoler Proteomics Center, Faculty of Biology, Technion-Israel Institute of Technology, Haifa 32000, Israel

[5]Department of Pathology, Rambam Health Care Campus, Haifa 31096, Israel

[6]Department of Chemistry, Ben-Gurion University of the Negev, Beer Sheba 84105, Israel

[7]The Schulich Faculty of Chemistry, Technion Israel Institute of Technology, Haifa 32000, Israel

[8]Department of Immunology and Cancer Research

[9]Department of Pathology

Institute for Medical Research Israel-Canada (IMRIC), Hebrew University-Hadassah Medical School, Jerusalem 91120, Israel

[10]Protein Metabolism Medical Research Center

[11]Department of Biomedical Sciences

College of Medicine, Seoul National University, Seoul 110-799, South Korea

[12]Department of Otolaryngology, Head and Neck Surgery, Carmel Medical Center, Haifa 34367, Israel

[13]Co-first author

*Correspondence: aaroncie@tx.technion.ac.il

http://dx.doi.org/10.1016/j.cell.2015.03.001

SUMMARY

NF-κB is a key transcriptional regulator involved in inflammation and cell proliferation, survival, and transformation. Several key steps in its activation are mediated by the ubiquitin (Ub) system. One uncharacterized step is limited proteasomal processing of the NF-κB1 precursor p105 to the p50 active subunit. Here, we identify KPC1 as the Ub ligase (E3) that binds to the ankyrin repeats domain of p105, ubiquitinates it, and mediates its processing both under basal conditions and following signaling. Overexpression of KPC1 inhibits tumor growth likely mediated via excessive generation of p50. Also, overabundance of p50 downregulates p65, suggesting that a p50-p50 homodimer may modulate transcription in place of the tumorigenic p50-p65. Transcript analysis reveals increased expression of genes associated with tumor-suppressive signals. Overall, KPC1 regulation of NF-κB1 processing appears to constitute an important balancing step among the stimulatory and inhibitory activities of the transcription factor in cell growth control.

INTRODUCTION

The NF-κB family of transcription factors is involved in regulation of a variety of genes that control the immune and inflammatory response, cell survival and death, proliferation, and differentiation. Recently—150 years after Rudolf Virchow discovered the infiltration of tumors with leukocytes and proposed a linkage between chronic inflammation and malignant transformation—it has been shown that the mechanism(s) that underlies this linkage is mediated largely by the NF-κB family of transcription factors (Ben-Neriah and Karin, 2011; DiDonato et al., 2012). NF-κB is overexpressed in numerous tumors. It upregulates expression of anti-apoptotic genes such as IAPs, cell-cycle promoters, and growth factors and their receptors (DiDonato et al., 2012). Nevertheless, in some cases NF-κB was shown to display strong tumor-suppressive characteristics (Perkins, 2012; Pikarsky and Ben-Neriah, 2006). For example, it is involved in regulation of activation-induced apoptosis of T lymphocytes (Ivanov et al., 1997) and in inducing cell-cycle arrest and cell death caused by repression of Bcl2, XIAP, Bcl-X_L, Cyclin D1, and c-Myc that occurs after cell damage. The arrest and death are mediated by p52 dimers (Barré et al., 2010; Barré and Perkins, 2007). Also, it was shown that NF-κB1$^{-/-}$ cells accumulate alkylator-induced mutations, and NF-κB1$^{-/-}$ mice develop more lymphomas following alkylating agent-induced DNA damage, again suggesting that NF-κB1 can act as a tumor suppressor (Voce et al., 2014).

The family members are mostly heterodimers where one of the subunits—p52 or p50—is the product of limited, ubiquitin- and proteasome-mediated processing of a longer (and inactive) precursor, p100 or p105, respectively (Betts and Nabel, 1996; Fan and Maniatis, 1991; Palombella et al., 1994). The other subunit is typically a member of the Rel family of proteins (RelA-p65, RelB, or c-Rel). At times, p50 and p52 can generate homodimers

that cannot act as transcriptional activators since they lack a transactivation domain present in the Rel proteins. In unstimulated cells, the NF-κB dimers are sequestered in the cytosol attached to ankyrin repeats (ARs) of IκB inhibitory proteins (IκB, Bcl3, p100, and p105). A broad array of extracellular signals stimulate degradation of the IκB proteins, resulting in translocation of the dimers to the nucleus where they initiate different transcriptional programs (Rahman and McFadden, 2011).

Proteasomal processing of p105 occurs under both basal conditions and following stimulation and requires prior ubiquitination (Cohen et al., 2004; MacKichan et al., 1996). One element that was shown to be important in the processing is a long Gly-Ala repeat in the middle of p105 that may serve as a proteasomal "stop signal" (Lin and Ghosh, 1996). In addition to processing, p105 can also undergo complete degradation, releasing NF-κB dimers anchored to its C-terminal ARs domain. Following stimulation, p105 is phosphorylated on serine residues 927 and 932 by IκB kinase (IKKβ) (Salmerón et al., 2001). This modification recruits the beta-Transducin Repeat Containing Protein (βTrCP) E3 (Orian et al., 2000), resulting in complete degradation of the molecule (Heissmeyer et al., 2001). The ligase(s) involved in processing of p105 under basal conditions as well as following stimulation has remained elusive.

In the present study, we identified KIP1 ubiquitination-promoting complex (KPC) as the Ub ligase that is involved in both basal and signal-induced processing of p105. KPC is a heterodimer made of KPC1 (*RNF123*) and KPC2 (*UBAC1*). It was shown to degrade the cyclin-dependent kinase inhibitor p27Kip1 in the G1 phase of the cell cycle (Kamura et al., 2004). KPC1 is a RING-finger protein that serves as the ligase. KPC2 interacts with ubiquitinated proteins and with the proteasome via its two Ub-associated domains and a Ub-like domain, acting as a shuttle that promotes the degradation of p27Kip1. It was also shown to stabilize KPC1 (Hara et al., 2005).

RESULTS

Identification of KPC1 as the p105 Ub Ligase

One of the still missing links in the Ub-mediated activation pathway of NF-κB is the identity of the ligase that ubiquitinates p105, resulting in its proteasomal processing to the p50 active subunit. To identify the ligase, we sequentially fractionated rabbit reticulocyte lysate using different chromatographic principles (Figure 1Ai). Each fraction along the different steps was monitored for E3 activity in a cell-free reconstituted conjugation assay containing in vitro translated ^{35}S-labeled p105 as a substrate (Figure 1Aii). To avoid ubiquitination by the βTrCP ligase, we used p105S927A mutant that cannot be phosphorylated by IKKβ and therefore cannot bind this E3. Employing mass spectrometric analysis, peptides derived from the KPC Ub ligase were identified in active fractions along the three last chromatographic steps. In the last step of purification (heparin), we identified 58 KPC1 peptides and seven KPC2 peptides covering 43.21% and 19.8% of the open reading frames, respectively (Figure 1B). Because of lack sequence information on rabbit KPC2, we used the sequence of the mouse protein to demonstrate the coverage map. The changes between the two species are negligible (but shown).

To test directly the role of KPC in p105 ubiquitination and processing, we established a cell-free conjugation assay using labeled p105 as a substrate and purified KPC1 or its catalytically inactive species (mutated in the RING domain) KPC1I1256A as the ligase. The wild-type (WT) ligase catalyzed conjugation of p105, whereas the inactive ligase did not (Figure 2A). It appears that KPC1 activity is specific to p105, as it scarcely modifies p100 that is highly homologous to p105 and also undergoes limited proteasomal processing, most probably by a different ligase (Figure S1A).

To demonstrate the ability of KPC1 to modify p105 in cells, we overexpressed Flag-p105 along with HA-Ub in HEK293 cells, in which KPC1 was either silenced (Figure 2B, lane 1), or overexpressed (Figure 2B, lanes 2 and 3). Immunoprecipitation of p105 revealed that it is sparsely ubiquitinated in the absence of the ligase, and ubiquitination is increased significantly following overexpression of KPC1 (Figure 2Bi; immunoprecipitation [IP], compare lanes 1 and 2). Furthermore, we found that p105 binds to KPC1 and co-immunoprecipitates with it (Figure 2Biii; IP, lane 2). In addition, we demonstrated that endogenous KPC1 interacts with endogenous p105 (Figure S1B).

KPC1 Promotes Basal and Signal-Induced Processing of p105

To demonstrate the involvement of KPC1 in p105 processing, we silenced its expression in cells using small interfering RNA (siRNA). As can be seen in Figure 2C, the silencing of KPC1 decreased the amount of p50 generated from p105. In a different experiment, we expressed in HEK293 cells FLAG-p105 along with Myc-KPC1 or Myc-KPC1I1256A. Less p50 was generated in the presence of the KPC1 mutant (Figure S1C).

As noted, processing of p105 occurs also following stimulation. It was interesting to study whether KPC1 can promote p105 processing under these conditions as well. Therefore, we tested the generation of p50 from p105 following expression of constitutively active IKKβ (IKKβS176,180E) in the presence (endogenous) or absence (silenced) of KPC1. As expected, the stimulation increased the processing of p105 (compare Figure 2D to Figure 2C; control siRNA). Silencing of KPC1 significantly decreased the generation of p50 following stimulation, strongly suggesting a role for KPC1 in signal-induced processing (Figure 2D). It is known that under the influence of the kinase, the precursor was not only processed but also degraded to a significant extent (compare Figure 2D to Figure 2C and note in particular the decreasing amount of p105 + p50 remained along time following stimulation). It should be noted that the degradation rate of p105 following stimulation was significantly higher in cells that lack KPC1 (Figure 2D). It is possible that the processing of p105 mediated by KPC1 and its degradation mediated by βTrCP occur in parallel. When one process is inactivated, the other becomes dominant. The influence of KPC1 on signal induced-processing of p105 appears to be specific, as its silencing does not affect the processing of p100 following NF-κB-inducing kinase (NIK) expression (Figure S1D).

In all these experiments, we used exogenously expressed p105. To demonstrate the effect on endogenous p105, we used the human haploid cell line HAP1 in which the single allele of KPC1 or KPC2 were knocked out using the Crispr-CAS

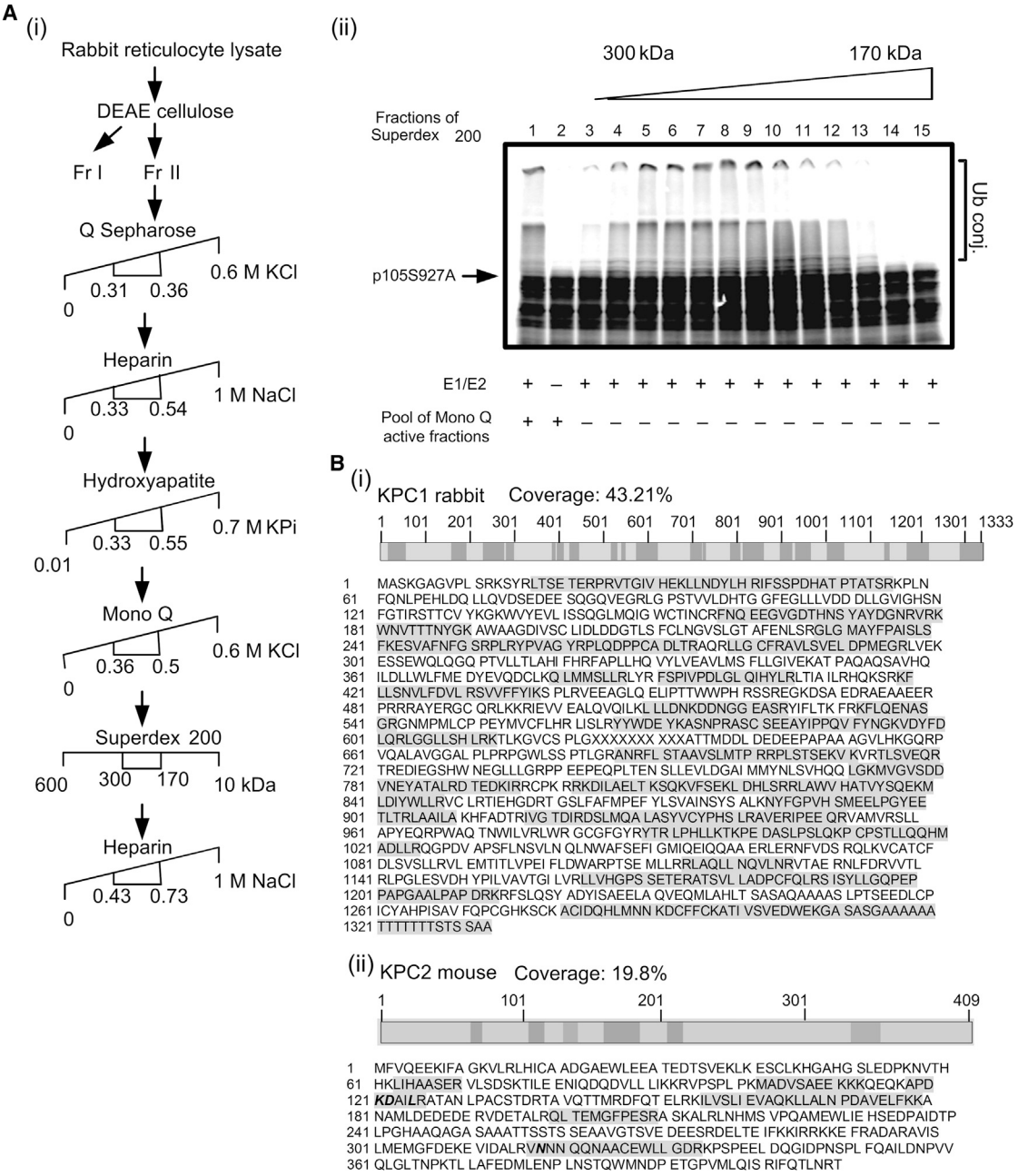

Figure 1. Purification and Identification of the p105 Ub Ligase

(A) (i) Scheme of the chromatographic resolution of Fraction II monitoring the E3 ligating activity toward p105. Numbers represent salt concentrations (M) or molecular weight (kDa) at which the ligating activity was eluted from the respective columns. Fr II, Fraction II. (ii) E3 conjugating activity profile along the fractions resolved by the Superdex 200 gel filtration column. In vitro translated and ^{35}S-labeled p105S927A was ubiquitinated in a reconstituted cell-free system in the presence of the resolved fractions.

(B) (i) Peptide coverage map of rabbit KPC1. The peptides were identified through mass spectrometric analysis of the E3-containing fractions resolved by the last, Heparin-based column. (ii) Peptide coverage map of mouse KPC2. The peptides were identified through mass spectrometric analysis of the E3-containing fractions resolved by the last, Heparin-based column. Residues marked in bold and italics denote differences in sequence between mouse and rabbit.

technology. Elimination of KPC1 or KPC2 (that stabilizes KPC1 [Hara et al., 2005]; note that removal of KPC2 results in a significant decrease in the level of KPC1; Figure 2E) decreased the generation of p50 both in the presence or absence of TNFα (Figure 2E). In contrast, the level of p65 was not affected. The finding that p50 is still present, albeit in a decreased level, in the KPC1 KO cells, may be due to the activity of another, yet to be identified ligase, and/or to co-translational processing of

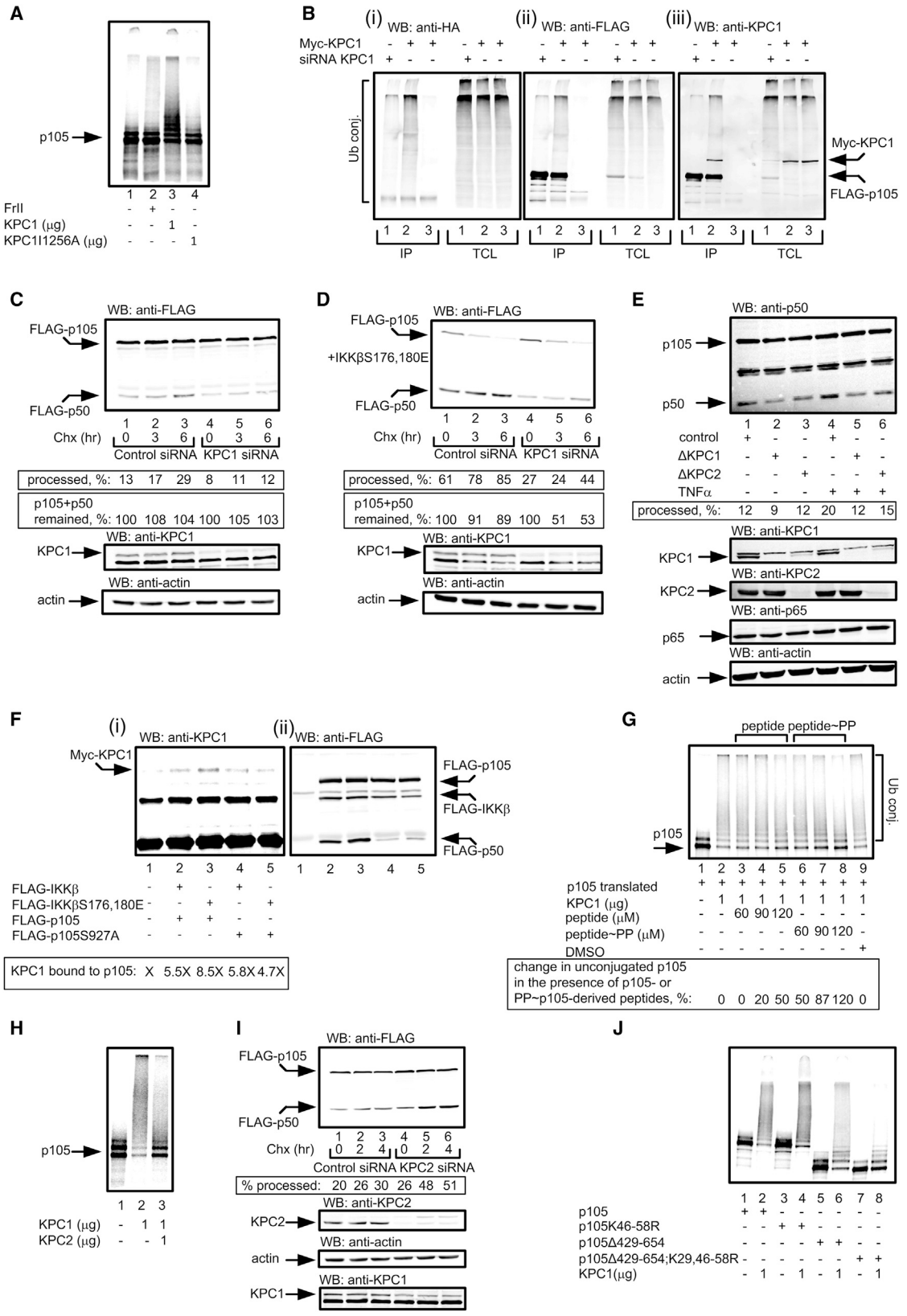

(legend on next page)

the nascent peptide that occurs before completion of the p105 precursor synthesis (Lin et al., 1998). It should also be noted that the effect of KPC1 on p50 generation is significantly more pronounced in tumors growing in mice than in cultured cells (see below).

Our finding that KPC1 mediates processing under both basal and stimulated conditions prompted us to dissect the mechanism involved. We monitored the interaction between KPC1 and p105 under basal and stimulated conditions and found that expression of constitutively active IKKβ results in increased interaction between the two as assayed by co-immunoprecipitation (Figures 2F and S1E). The finding that the interaction of p105S927A with KPC1 is not affected by IKKβ (Figure 2Fi, lanes 4 and 5) attests to the specificity of the effect of IKKβ in phosphorylating a specific Ser residue (927) in p105. As expected, we found that ubiquitination of phosphorylated p105 by KPC1 is stronger compared to that of the non-phosphorylated species (Figure S1F).

To further confirm that KPC1 interacts more efficiently with phosphorylated p105, we designed an experiment in which we competed on the binding of p105 to the ligase with a synthetic phosphorylated peptide derived from the p105 IKKβ-phosphorylation site. The phosphorylated peptide inhibited ubiquitination of p105 by KPC1 to a larger extent compared with its non-phosphorylated species, both in a crude system and in a system made of purified components (Figures 2G and S1G, respectively).

Role of KPC2 in KPC1-Mediated p105 Ubiquitination and Processing

At that point, it was important to study the role of KPC2, the partner of KPC1 in the heterodimeric ligase complex, in p105 modification and processing. We noted that its addition to a reconstituted cell-free system decreases significantly the ubiquitination of p105 by KPC1 (Figure 2H). This was true also when p105 was purified by a specific antibody, ruling out a possible effect of other components present in the mixture in which the labeled p105 was translated (Figure S2Ai). To rule out that the reduced ubiquitination of p105 in the presence of KPC2 is due to a possible deubiquitinating activity of the protein, we added it to the cell-free ubiquitination system after KPC1, when most of the ubiquitination reaction was completed. It had no effect on the conjugates pattern (Figure S2Aii). The interference of KPC2 in chain formation appears to be specific to KPC1 and p105, as it did not affect the ligase activity of E6-AP toward RING1B^{I53S} (Zaaroor-Regev et al., 2010) (Figure S2B).

Importantly, in correlation with the suppressive effect of KPC2 on KPC1-mediated ubiquitination of p105, silencing of KPC2

Figure 2. p105 Is a Substrate of KPC1 in a Cell-free System and in Cells, Both under Basal Conditions and following Signaling

(A) Ubiquitination of in vitro translated and ^{35}S-labeled p105 by Fraction II and purified KPC1-FLAG-TEV-6xHIS or KPC1I1256A-FLAG-TEV-6xHIS in a reconstituted cell-free system. Fr II, Fraction II.

(B) KPC1 ubiquitinates p105 in cells. HEK293 cells that were transfected with siRNA to silence KPC1 (lane 1) or with control siRNA (lanes 2 and 3), were also transfected with cDNAs coding for FLAG-p105 (lanes 1 and 2), HA-Ub (lanes 1–3), and Myc-KPC1 (lanes 2 and 3). FLAG-p105 and its conjugates were immunoprecipitated from the cell lysates using immobilized anti-FLAG (IP; lanes 1–3), resolved via SDS-PAGE, and visualized using anti-HA (Bi) or anti-FLAG (Bii). KPC1 was visualized using a specific antibody to the protein (Biii). Ten percent of total cell lysates (TCL; lanes 1–3) were analyzed for expression of FLAG-p105, HA-Ub or Myc-KPC1, using anti-HA (Bi), anti-FLAG (Bii), or anti-KPC1 (Biii), respectively. IP, immunoprecipitation; WB, western blot.

(C) Silencing of KPC1 affects basal processing of p105. HEK293 cells were transfected with control siRNA (lanes 1–3) or siRNA to silence KPC1 (lanes 4–6). After 24 hr, cells were transfected with cDNAs coding for FLAG-p105. Processing of p105 was calculated as the ratio between the amount p50 at the specified time and the sum of p50 + p105 at time zero (in order to disregard degradation of p105 in our calculations), multiplied by 100%. The amount of p50 + p105 remained (reflecting degradation along time) was calculated as the sum of p50 + p105 measured at the relevant time point, divided by the sum of p50 + p105 at time zero, multiplied by 100%.

(D) Silencing of KPC1 inhibits signal-induced processing of p105. HEK293 cells were transfected with control siRNA (lanes 1–3) or siRNA that targets KPC1 (lanes 4–6). After 24 hr, cells were transfected with cDNAs coding for FLAG-p105 and IKKβS176,180E. Twenty-four hours after transfection (in the experiments depicted under C and D), cycloheximide was added for the indicated times, and cells were lysed, resolved via SDS-PAGE, and proteins visualized using anti-FLAG, anti-KPC1 or anti-actin. Processing and degradation were assessed as described under (C). Chx, cyclohexamide. Actin was used to ascertain equal protein loading.

(E) Deletion of KPC1 or KPC2 genes inhibits basal and TNFα-induced processing of endogenous p105. Lysates were prepared from HAP1 control or HAP1 cells knocked out for the genes coding for KPC1 or KPC2. The lysates were resolved via SDS-PAGE, and proteins were visualized using anti-NF-κB1, anti-KPC1, anti-KPC2, anti-p65, or anti-actin. The amount of p105 processed was calculated as the ratio between the generated p50 and the sum of p50 + p105, multiplied by 100%.

(F) The interaction between p105 and KPC1 increases following signaling. HEK293 cells were transfected with cDNAs coding for FLAG-p105 (lanes 2 and 3) or FLAG-p105S927A (lanes 4 and 5) along with Myc-KPC1 (lanes 1–5) and FLAG-IKKβ (lanes 2 and 4) or FLAG-IKKβS176,180E (lanes 3 and 5). FLAG-p105 and FLAG-p105S927A were immunoprecipitated from the cell lysate using immobilized anti-FLAG (lanes 1–5), and the bound KPC1 was visualized with anti-KPC1 (Fi). Immunoprecipitated p105s were visualized using anti-FLAG (Fii).

(G) A phosphorylated peptide corresponding to the signaled sequence in p105 inhibits its ubiquitination. In vitro translated and ^{35}S-labeled p105 was ubiquitinated by purified KPC1-FLAG-TEV-6xHIS (lanes 2–9) in a reconstituted cell-free system in the presence of a phosphorylated peptide derived from the signaled sequence of p105 (lanes 6–8), or in the presence of its non-phosphorylated counterpart (lanes 3–5). Presented is the change (in %) of unconjugated p105 remained following addition of increasing concentrations of the peptides (compared to a system to which a peptide was not added; lane 2).

(H) KPC2 attenuates ubiquitination of p105 by KPC1. Ubiquitination of in vitro translated and ^{35}S-labeled p105 by purified KPC1-FLAG-TEV-6xHIS in the presence or absence of HIS-KPC2 was carried out in a cell-free reconstituted system.

(I) KPC2 attenuates processing of p105 in cells. HEK293 cells were transfected with control siRNA (lanes 1–3) or siRNA to silence KPC2 (lanes 4–6). After 24 hr, cells were transfected with cDNAs coding for FLAG-p105 and generation of p50 was monitored 24 hr later. Processing of p105 was calculated as described under (C).

(J) KPC1 modifies lysine residues in the C-terminal segment of p105. In vitro-translated and ^{35}S-labeled WT and the indicated p105 mutants were subjected to ubiquitination by purified KPC1-FLAG-TEV-6xHIS in a reconstituted cell-free system.

See also Figures S1 and S2.

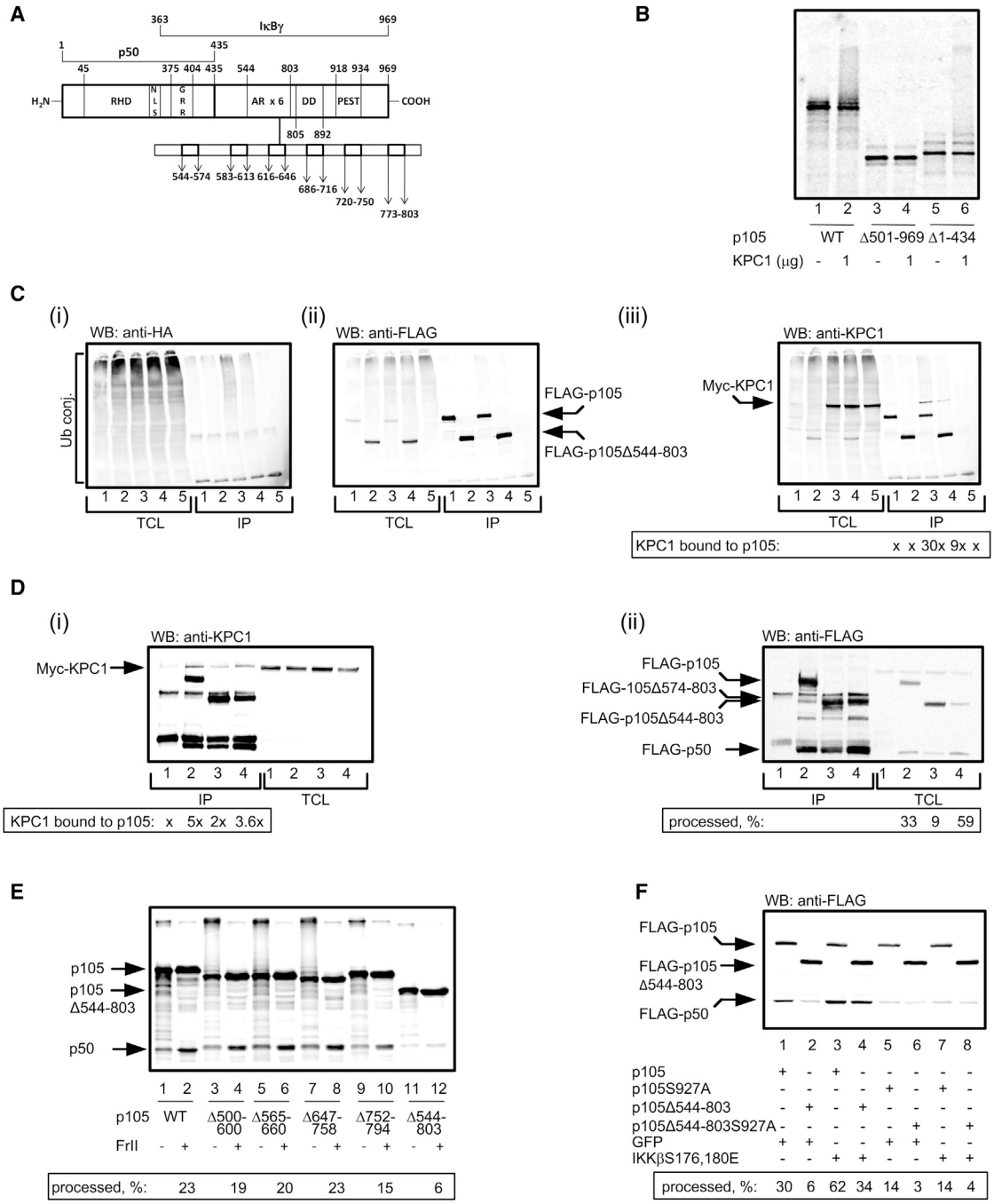

Figure 3. KPC1-Dependent Ubiquitination and Processing of p105 Require the ARs of p105

(A) Schematic representation of p105 domains. Numbers denote the respective residue along the protein sequence. RHD, Rel homology domain; NLS, nuclear localization signal; GRR, glycine rich repeat; AR, ankyrin repeats (all six of them are marked).

(B) The ARs-containing C-terminal half of p105 is ubiquitinated by KPC1. In vitro-translated and ^{35}S-labeled p105, p105Δ501-969 or p105Δ1-434 were subjected to ubiquitination by purified KPC1-FLAG-TEV-6xHIS in a reconstituted cell-free system.

(C) The ARs of p105 are essential for binding of KPC1 and for its ubiquitination by the ligase in cells. HEK293 cells that were transfected with siRNA to silence KPC1 (lanes 1 and 2) or with control siRNA (lanes 3–5), were also transfected with cDNAs coding for FLAG-p105 (lanes 1 and 3), p105Δ544-803 (lanes 2 and 4), HA-Ub (lanes 1–5), and Myc-KPC1 (lanes 3–5). The different FLAG-p105 species and their conjugates were immunoprecipitated from the cell lysates by immobilized anti-FLAG (IP; lanes 1–5).

(D) KPC1 interacts with a single AR in p105. HEK293 cells were transfected with cDNAs coding for FLAG-p105 (lane 2), FLAG-p105Δ544-803 (lane 3), or FLAG-p105Δ574-803 (lane 4), along with Myc-KPC1 (lanes 1–4). The different FLAG-p105 species were immunoprecipitated from the cell lysates using immobilized anti-FLAG (IP; lanes 1–4).

(legend continued on next page)

increased the formation of p50 (Figure 2I). That, despite the fact that the short-term silencing reduced partially the level of KPC1 via its effect (or absence thereof) on the stabilization of the ligase (Figure 2I; note the change in the level of KPC1 following KPC2 silencing).

Identification of the Ub Anchoring Sites on p105 Modified by KPC1

We have already shown that multiple lysines in the C-terminal segment of p105 are required for its ubiquitination and processing (Cohen et al., 2004; Kravtsova-Ivantsiv et al., 2009) in crude extracts. It was therefore important to show that this is true also for KPC1. Progressive removal of all lysine residues from the C-terminal segment (Figure S2C) resulted in corollary decrease in conjugation of p105 by KPC1 in a cell-free assay (Figure 2J) and in processing of the precursor in cells (Figure S2D).

The C-Terminal ARs of p105 Are Necessary for Its Interaction with KPC1 and for Its Subsequent Ubiquitination and Processing

p105 harbors several domains: REL homology domain (RHD), nuclear localization signal (NLS), and a glycine rich repeat (GRR) in its N-terminal segment, and ARs, death domain (DD), and a PEST (proline, glutamate, serine, and threonine) sequence in the C-terminal segment (Figure 3A). We examined which of these domains is necessary for ubiquitination by KPC1. As can be seen in Figure 3B, removal of the C-terminal segment abolished altogether conjugation in a cell-free system, whereas removal of the N-terminal segment had no effect. Subsequently we found that removal of all six ARs (p105Δ544-803) affected significantly the ubiquitination of p105 by KPC1 (Figure S3A, compare lanes 2 and 12). Partial deletion of the repeats affected conjugation only slightly (compare lane 2 to lanes 4, 6, 8, and 10).

Similar results were obtained in experiments carried out in cells. Overexpression of KPC1 increased the ubiquitination of WT p105, but much less so of p105 that lacks all its ARs (Figure 3Ci; IP, compare lane 4 to lane 3). Importantly, in parallel, we observed also a decrease in the interaction between the ARs'-truncated p105 and its ligase compared to WT p105 (Figure 3Ciii; IP, compare lanes 4 and 3).

To rule out the possibility that the decrease in ubiquitination of p105 that lacks all its ARs is due to removal of the eight lysine residues in the repeats, we generated a mutant p105 in which all these lysines were substituted by arginines. The ubiquitination of the K to R mutant as well as its interaction with KPC1, were similar to that of WT p105 (Figures S3Bi and ii, respectively). An interesting question relates to the number of ARs necessary for ubiquitination and processing of p105. We constructed a p105 mutant where all ARs except one have been deleted (p105Δ574-803). The single remaining AR was sufficient to bind KPC1 and to promote processing similar to that observed for WT p105 (Figure 3D). Thus, it appears that the ARs are redundant with relation to binding of KPC1.

Last, it was important to demonstrate whether the ARs-dependent ubiquitination increases the processing of p105. As can be seen in Figure 3E, mutant p105 that lacks all ARs, is processed much less efficiently compared to the WT species and to one lacking only some of the repeats (compare lane 12 to lanes 2, 4, 6, 8, and 10). A similar result was obtained also in cells (Figure 3F, lanes 1 and 2). Mutant p105 in which all lysine residues in the ARs were substituted with arginines (FLAG-p105K8R), is processed similarly to WT p105 (Figure S3C, lane 3), strongly suggesting that the ARs are required for the binding, ubiquitination, and processing of p105, but do not serve as ubiquitination sites essential for processing.

It appears that the ARs are also involved in signal-induced processing of p105, as their removal significantly decreased IKKβ-mediated generation of p50 (Figure 3F, compare lane 4 to lane 3). As expected, FLAG-p105S927A and FLAG-p105S927AΔ544-803 did not respond to IKKβ-mediated phosphorylation (Figure 3F, lanes 7 and 8).

Overexpression of KPC1 or p50 Suppresses Tumor Growth

Since NF-κB dimers are known to affect cell survival, proliferation, and tumor progression, it was interesting to study the outcome of KPC1 on cell growth. Initially, we monitored the influence of overexpressed KPC1 on anchorage-independent growth in MB-MDA 231, U2OS, and U87-MG cells, and found that it inhibits colony formation by 36%, 32%, and 52%, respectively, compared to controls (Figures 4A–4C). Importantly, this effect was abrogated in cells overexpressing the inactive ligase species KPC1I1256A, suggesting that the inhibitory effect is due to the ligase activity (Figure 4C). Cells expressing p50 showed an even stronger inhibition of colony formation (73% for both MB-MDA 231 and U87-MG cells; Figures 4A and 4C), strongly suggesting that the effect of the ligase is mediated through its activity on p105, resulting in excessive generation of p50. Supporting the linkage is the finding that silencing of p105 abrogated the strong suppressive effect of KPC1: the number of colonies formed using cells that overexpress KPC1 in the absence of p105 was 7.5-fold larger than that formed in its presence (Figure 4D). It was important to study whether the growth suppressive effect of KPC1 and p50 is not due to induction of apoptosis. Thus, we stained U87-MG cells that overexpress these proteins for cleaved caspase 3. As can be seen in Figure S4, we could not detect the apoptotic marker. For that

(E) p105 that lacks its ARs is processed less efficiently in a cell-free system. The different ^{35}S-labeled p105 species were processed in a cell-free reconstituted system in the presence or absence of Fraction II as indicated. Fr II, Fraction II.

(F) Deletion of the ARs of p105 affects both its basal and signal-induced processing. HEK293 cells were transfected with cDNAs coding for FLAG-p105, FLAG-p105Δ544-803, FLAG-p105S927A, or FLAG-p105S927AΔ544-803 along with either GFP or IKKβ as indicated.

In (C), (D), and (F), proteins were resolved via SDS-PAGE, blotted onto nitrocellulose membrane, and p105 and p50 were detected using anti-FLAG, KPC1 was detected using anti-KPC1, and Ub conjugates were detected using anti-HA. Ten percent of the total cell lysates (TCL) were analyzed for the expression of proteins. The SDS-PAGE-resolved labeled proteins in the experiments shown in (B) and (E) were visualized using PhosphorImaging. Processing was assessed as described under Figure 2E.

See also Figure S3.

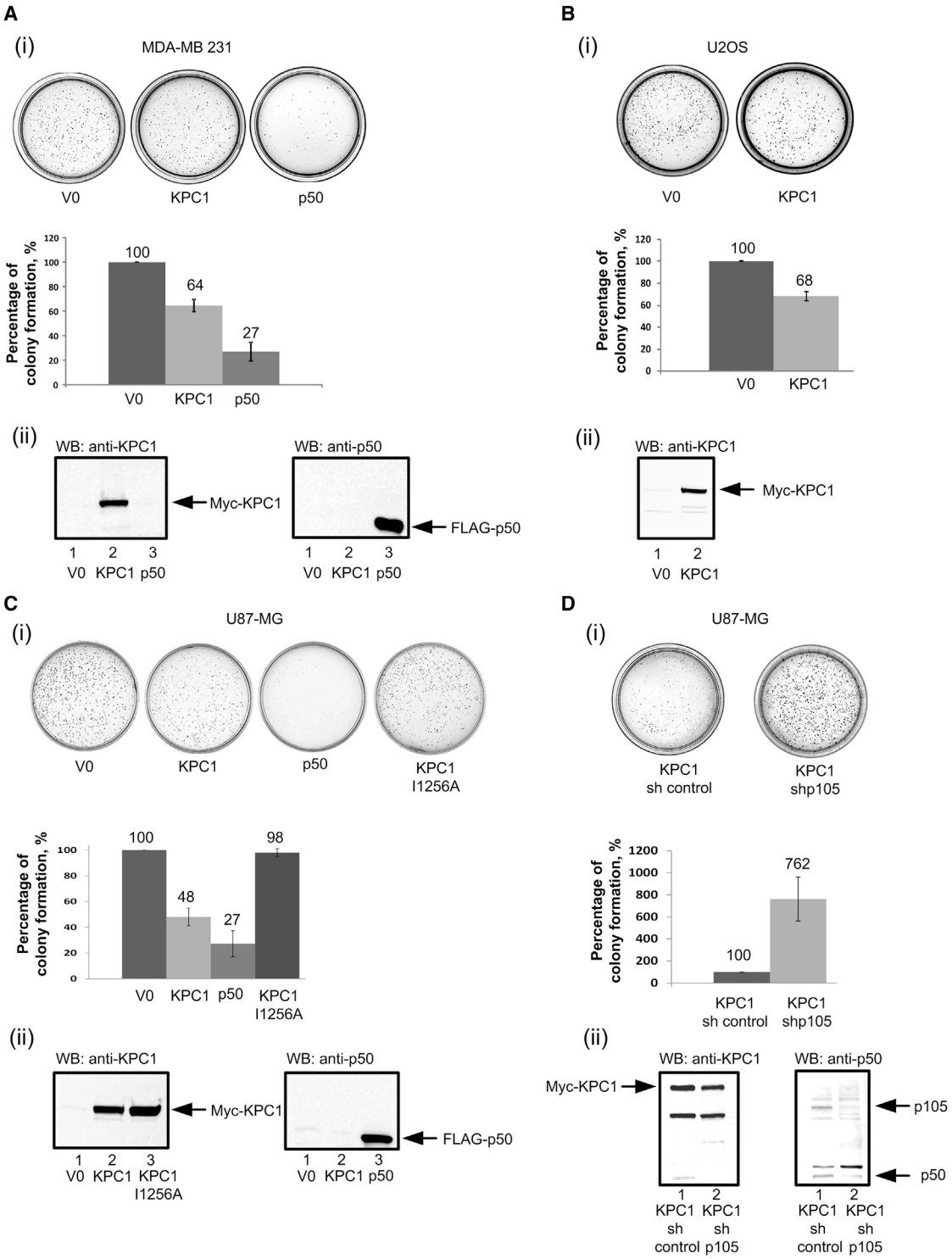

Figure 4. KPC1 and p50 Suppress Anchorage-Independent Growth of Cells

Suppression of colony formation by overexpressed KPC1 or p50 in MDA-MB 231 (Ai), U2OS (Bi), and U87-MG (Ci and Di) cells. Cells were stably transfected with V0, or with cDNAs that code for Myc-KPC1, Myc-KPC1I1256A or FLAG-p50, or with cDNA coding for Myc-KPC1 along with control shRNA or shRNA to silence p105, as indicated, and were seeded on soft agar plates. After 3 weeks, the colonies were stained with 0.05% crystal violet. Data derived from five experiments (±SEM) are presented graphically. Expression of KPC1, KPC1I1256A, p50, and p105 is shown in (Aii), (Bii), (Cii), and (Dii).

See also Figure S4.

experiment, it was also important to demonstrate that the suppressive effect of KPC1 and p50 is not due to some non-specific effect of the overexpression of the proteins. The unleashing of growth in the presence of overexpressed KPC1 but in the absence of p105 (Figure 4D), strongly suggests that the effect of KPC1 is indeed specific.

These observations prompted us to study the effect of KPC1 in a tumor model in mice. We generated xenografts stably overexpressing V0, KPC1, KPC1I1256A, or p50. Both the growth rate and weights of tumors expressing KPC1 and p50 were significantly smaller compared to those that harbor V0 or KPC1I1256A (Figures 5Ai and 5Aiii for xenografts derived from U87-MG cells, and Figure 5Aii for xenografts derived from MDA-MB 231 cells). Importantly, in tumors that overexpress KPC1, the level of p50 is significantly higher compared with tumors that express V0 (Figure 5Aiv), suggesting again a direct linkage between the KPC1 ligase activity and increased generation of p50. Interestingly, in tumors that overexpress KPC1 or p50, we also observed a significant decrease in the level of p65 (Figure 5Aiv). This finding raises the possibility that a different NF-κB transcription factor is generated under the influence of KPC1, possibly a p50 homodimer (see Discussion). To demonstrate that there are indeed changes in NF-κB species in human tumor xenografts overexpressing KPC1 and p50, we used electrophoretic mobility shift assay (EMSA) to monitor the activity of the transcription factor. As can be seen in Figure S5A, there is a significant decrease in the ability of "canonical" NF-κB to bind its consensus DNA sequence following overexpression of KPC1 and even more so following overexpression of p50.

Of note, all the effects on tumor growth (reduction in colony formation, tumor growth rate, and weight) were more prominent in p50-expressing tumors than in their KPC1-overexpressing counterparts. This is not surprising, as p50 is the product of KPC1 activity, and its direct expression has a stronger effect.

The functional linkage between KPC1 and p50 can also be observed in staining of specific proliferation and differentiation markers in the mice-derived tumors. The overexpression of KPC1, but not of KPC1I1256A, results in increased appearance of nuclear NF-κB (Figure 5B), a significant decrease in the proliferation marker ki-67, and an increase in the glial fibrillary acidic protein (GFAP), a known glial cells differentiation marker. Suspecting that KPC1 stimulates apoptosis, we looked for an increase in cleaved caspase 3, however, there was no change in the levels of the active enzyme compared to control sections. Staining of p27Kip1—a suggested substrate of KPC1 (Kamura et al., 2004)—did not show any change in the protein level (Figure 5B). This may be due to the differences in the systems studied.

KPC1 Regulates Expression of a Subset of p50 Target Genes

We next analyzed the profile of gene expression in the tumors using RNA sequencing (RNA-seq) analysis of transcripts mapped to the human genome (http://www.ncbi.nlm.nih.gov/geo/query/acc.cgi?acc=GSE60530; Table S1). The altered gene expression patterns revealed a strong similarity between overexpression of p50 and KPC1 in U87-MG xenografts (correlation of 0.51, p value $< 10^{-300}$; Figure 6Ai), with 48 downregulated and 534 upregulated genes that were consistent and significant in all replicates (Figure 6Aii; Table S2). The relative transcript levels of selected genes that were shown to be significantly upregulated and downregulated in RNA-seq analyses, was corroborated by quantitative real-time PCR (qRT-PCR) (Figure S5B). Functional analysis revealed highly significant enrichment in glycosylated and extracellular matrix proteins, and upregulation of genes expressing proteins involved in cell-cell and cell-substrate adhesion, regulation of cell migration, cell junctions, vasculature development, wound healing, and cell-cell signaling (Figure 6Aiii), suggesting a re-establishment of "social" micro-environmental interactions in the p50- and KPC1-overexpressing glioblastoma tumors (Bonavia et al., 2011). Downregulated processes included a reduced response to hypoxia required for maintaining glioblastoma stem cells (Heddleston et al., 2009), as well as reduced positive regulation of cell migration (Figure 6Aiii). Of the consistently changed genes, 21 are known NF-κB targets (p value $< 3.4 \times 10^{-9}$; http://www.bu.edu/nf-kb/gene-resources/target-genes/). To further assess if the observed reduction in tumor size was the consequence of a reduction in proto-oncogenes and/or of an increased expression of tumor suppressor genes, we gathered gene annotations from various sources. Enrichment analysis on these gene annotations revealed a significant (p value $< 1.4 \times 10^{-18}$) increase in the expression of 40 tumor suppressor genes, with no significant change in other classes (Figure 6B).

Finally, we integrated functional annotation enrichment and protein-protein interactions for the differentially regulated genes, which revealed a dense network of upregulated genes revolved around a few downregulated ones, such as interleukin-6 (IL-6), interleukin-6 receptor (IL-6R), and vascular endothelial growth factor A (VEGFA) (Figure 6C; Data S1). We included KPC1 and NF-κB in this analysis to retrieve possible known interactions, although KPC1 had no known interactions with any of the differentially regulated genes. Closer look at the core interaction network (Figure 6C, inset magnification) that included NF-κB is most prominently annotated with "regulation of cell migration" genes. Most other core network genes are upregulated and include many well-known tumor-suppressor genes.

Taken together, our findings strongly suggest a model of KPC1/p50 driven glioblastoma tumor growth inhibition, that centers around downregulated high mobility group protein HMGI-C (HMGA2), lin-28 homolog A (LIN28), IL-6/IL-6R, and VEGFA, and upregulated tumor suppressors, which in combination control the tumor-microenvironment as well as glioblastoma stem cell maintenance.

Correlation between Expression of KPC1 and p50 in Human Tumoral and Normal Tissues

Finally, we examined the relationship between KPC1 and p50 in human tumors and normal tissues. Immunohistochemical staining of the two proteins (the two antibodies were shown to be specific; see Figure S6) revealed a high correlation between them in squamous cell carcinoma of head and neck (SCCHN, 52 sections; p value < 0.005; Figure 7Aii), breast cancer (105 sections; p value < 0.0001), and glioblastoma (192 sections; p value < 0.0017) (Figure 7Ai). It should be emphasized though

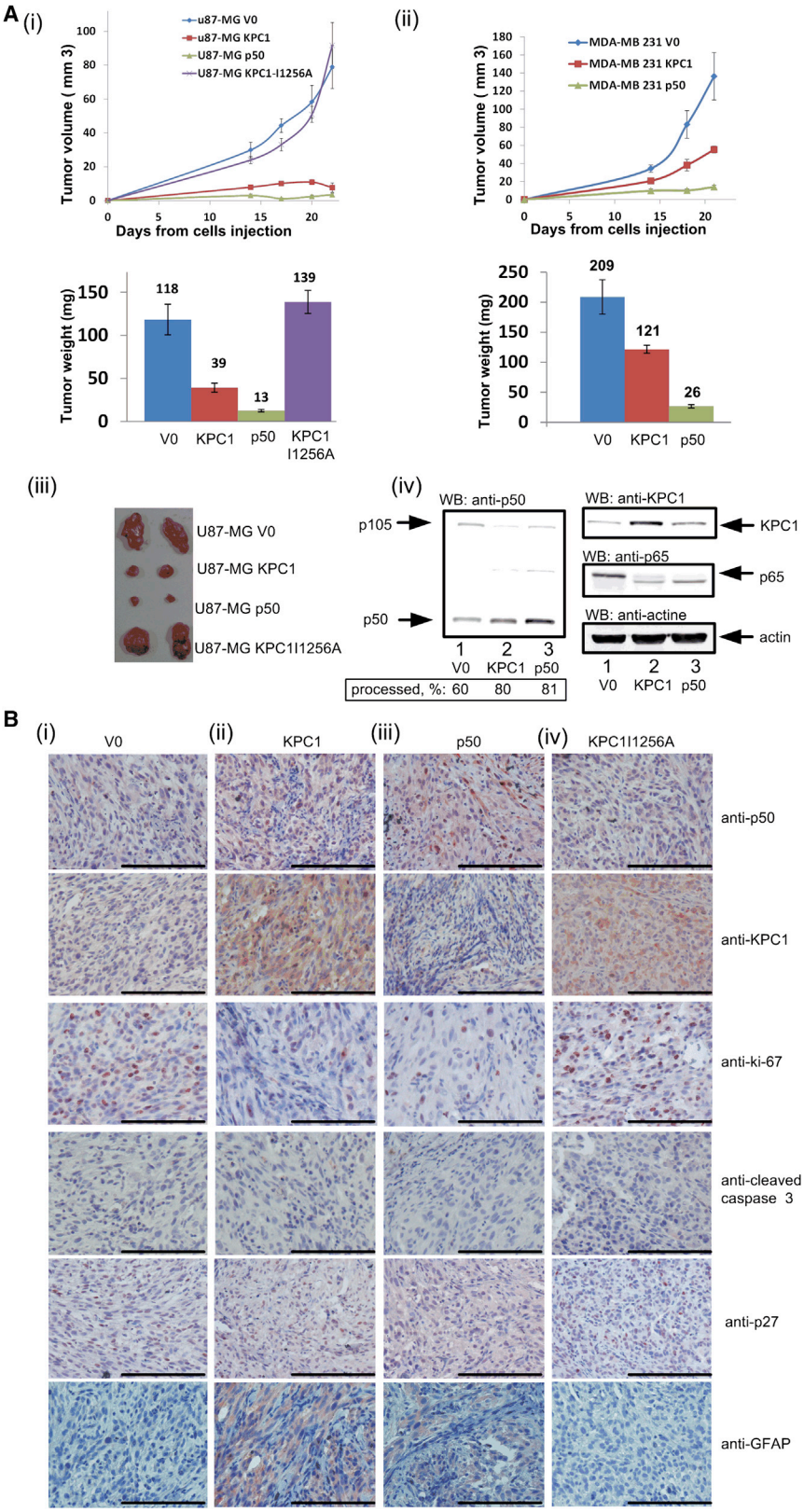

Figure 5. KPC1-Mediated Excessive Generation of p50 Inhibits Tumor Growth

(A) Growth rates and weights of tumor xenografts grown in mice, and derived from U87-MG (i) and MDA-MB 231 (ii) cells expressing V0, Myc-KPC1, and FLAG-p50. Data represent the mean of seven xenografts ± SEM (iii) Tumors derived from U87-MG cells 3 weeks after inoculation. (iv) Enhanced generation of p50 and disappearance of p65 in tumors that overexpress KPC1 and p50. Proteins were resolved via SDS-PAGE, blotted onto nitrocellulose membrane, and detected using the appropriate antibodies. Processing was assessed as described under Figure 2E.

(B) Immunohistochemical staining of p50, KPC1, ki-67, cleaved caspase 3, p27Kip1, and GFAP in xenografts of U87-MG cells stably expressing V0 (i), Myc-KPC1 (ii), FLAG-p50 (iii), or KPC1I1256A (iv).

All scale bars, 100 μm. Tumors were grown in mice and stained as described in the Experimental Procedures.

See also Figure S5.

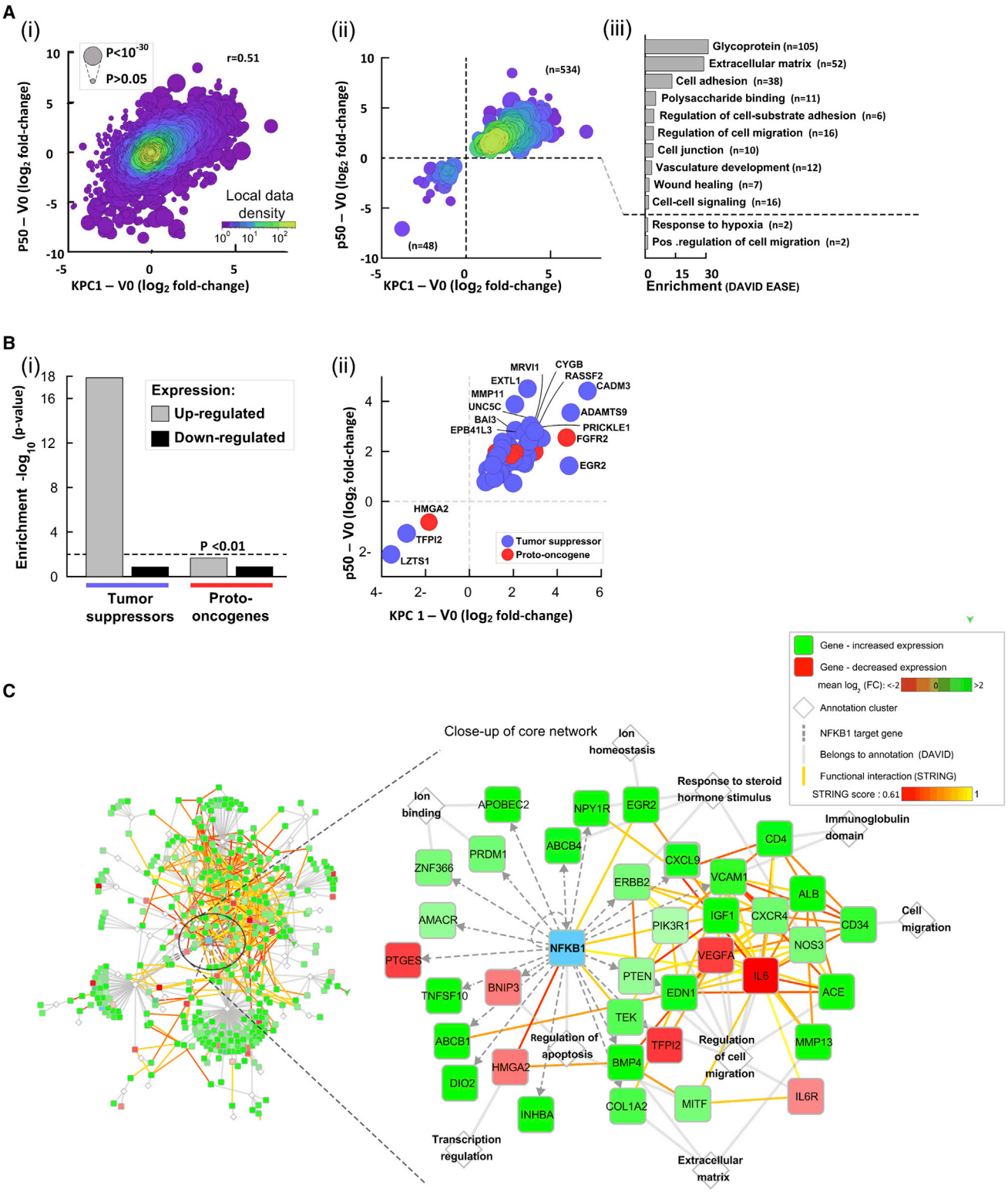

Figure 6. RNA Analysis of Glioblastoma Xenografts Expressing KPC1 and p50

(A) (i) Gene expression pattern as revealed by RNA-seq of U87-MG xenografts overexpressing either KPC1 or p50. Shown is log2-transformed fold-change in transcripts abundance against V0 control; dot size relates to the geometric mean significance over all experiments. (ii) Consistent downregulated and upregulated

(legend continued on next page)

that the linkage may be tumor-specific and not common to all patients with the "same" tumor.

To test the hypothesis that loss of KPC1 and nuclear p50 can be involved in the pathogenesis of malignant transformation, we analyzed the staining of the two proteins in SCCHN, breast cancer, and glioblastoma, and compared it to their staining in the normal parallel tissue. We observed a strong decrease in tumor samples stained for nuclear p50 compared to the healthy tissue (Figure 7B). As for KPC1, we observed a significant decrease in staining intensity (reflecting the amount of the protein) in cancerous compared to normal tissue in both SCCHN and glial cells, but not in breast cancer. Also, we noted a significant decrease in the number of tumor samples stained for KPC1 in SCCHN (Figure 7B). Taken together, these findings suggest that nuclear p50 is indeed a tumor suppressor lost in many malignancies. At least part of this p50 loss may be due to loss of KPC1 which catalyzes its formation, though this may not be common to all tumors.

DISCUSSION

The vast majority of substrates of the Ub proteasome system are completely degraded. One intriguing and exceptional case is that of the p105 precursor of NF-κB that can be either completely degraded or processed in a limited manner to yield the p50 active subunit of the transcription factor. The "decision-making" mechanism resulting in one of the two distinct processes has remained largely elusive. The βTrCP Ub ligase has been identified as the tagging enzyme involved in complete degradation of p105, whereas the ligase involved in processing has remained unknown. We have now identified the KPC complex as the putative p105-processing ligase (Figures 1, 2, and 3).

Now that the two E3s involved in degradation and processing of p105 have been identified, it is still not known why ubiquitination by one enzyme results in a completely different fate of p105 than ubiquitination by the other and what determines the timing of the two reactions. It is possible that the two ligases catalyze the formation of chains that differ in their anchoring sites, length, and/or internal linkages. These, in turn, affect the recognition and mechanism of action of the 26S proteasome. As for timing, it can be that different physiological conditions and/or the degree of saturation of the ARs with bound p50s are involved in the "decision-making" process of whether the molecule will be processed or destroyed completely.

Studying the biological implications of manipulating KPC1 revealed that it suppresses anchorage-independent growth in a manner that is dependent on its ligase activity and the presence of p105. A corollary strong tumor-suppressive effect was demonstrated in xenografts of human tumors (Figures 4, 5, and 6). This effect is caused probably by a significant increase in an entire set of tumor suppressors, some of them like the brain-specific protein cell adhesion molecule 3 (CADM3) (Gao et al., 2009), was found inactivated in glioblastoma.

An important question relates to the transcriptional mechanism by which KPC1 and p50 exert their tumor-suppressive effect. An obvious assumption is that the stoichiometric excess of p50 generated by KPC1 would generate mostly p50-p50 homodimers rather than the "canonical" tumorigenic p50-p65 heterodimers. In line with this finding is also the observation that p65 level is decreased in KPC1-overexpressing as well as in p50-overexpressing xenografts (Figure 5Aiv). It appears that each dimer of NF-κB family has unique and even opposing biological function(s) and regulates a distinct subset of downstream genes (Siggers et al., 2012). p50 homodimer is supposed to act as a transcriptional repressor because it does not contain a transactivation domain (May and Ghosh, 1997). However, studies in vitro have shown that p50 homodimer can interact with different transcriptional modulators, such as Bcl-3 (Fujita et al., 1993), p300 (Deng and Wu, 2003), or HMGA1/2 (Perrella et al., 1999) that are involved in chromatin remodeling. Disproportionate p50 may shift the composition of NF-κB dimers, resulting in overall tumor-suppressive effect. Indeed, following overexpression of KPC1 or p50, there is a decrease in the level of what is probably the "canonical" tumorigenic NF-κB (p50-p65; Figure S5A).

Importantly, we found a strong correlation between the expression of KPC1 and that of p50 in human tumors (Figure 7A). Moreover, we found a significant decrease in nuclear p50 and KPC1 staining intensity in tumors compared to non-malignant tissue (Figure 7B). This observation suggests that loss of nuclear p50 may trigger malignant transformation. In line with these findings are data collected in the Catalog Of Somatic Mutations in Cancer (COSMIC) that show a significantly greater number of common tumors (e.g., breast, lung, CNS, and uterine cervix) with decreased expression of KPC1 transcripts compared to those with high expression (http://cancer.sanger.ac.uk/cosmic/gene/analysis?ln=RNF123&ln1=RNF123&start=1&end=1315&coords=AA%3AAA&sn=&ss=&hn=&sh=&samps=1001&expn=over&expn=under&id=4185).

EXPERIMENTAL PROCEDURES

Materials, Plasmids, Expressed Proteins, and Cells

All materials (including plasmids and their construction, expression of proteins and their purification, and cultured cells and their manipulation), are described in the Extended Experimental Procedures.

Preparation and Fractionation of Crude Reticulocyte Lysate

Reticulocytes were induced in rabbits and lysates were prepared and fractionated over DEAE cellulose to Fraction I (unabsorbed material) and Fraction II

genes in the xenografts. Dot sizes are as in (i). (iii) Selected annotation clusters most enriched for either up- or downregulated genes (above or below dashed line, respectively).

(B) (i) Enrichment analysis of consistently upregulated and downregulated transcripts for tumor suppressors and proto oncogenes annotations. (ii) Expression differences for all tumor suppressors (blue) and proto oncogenes (red) from (i). Gene names of the strongest differentially regulated cancer-related genes are shown.

(C) Integrated analysis of functional annotation clusters and known functional and physical protein-protein interactions among all consistently upregulated and downregulated genes (green and red, respectively). NF-κB is shown in blue, and a close-up of the core interaction network surrounding NF-κB (inset) is displayed. See also Figure S5, Tables S1 and S2, and Data S1.

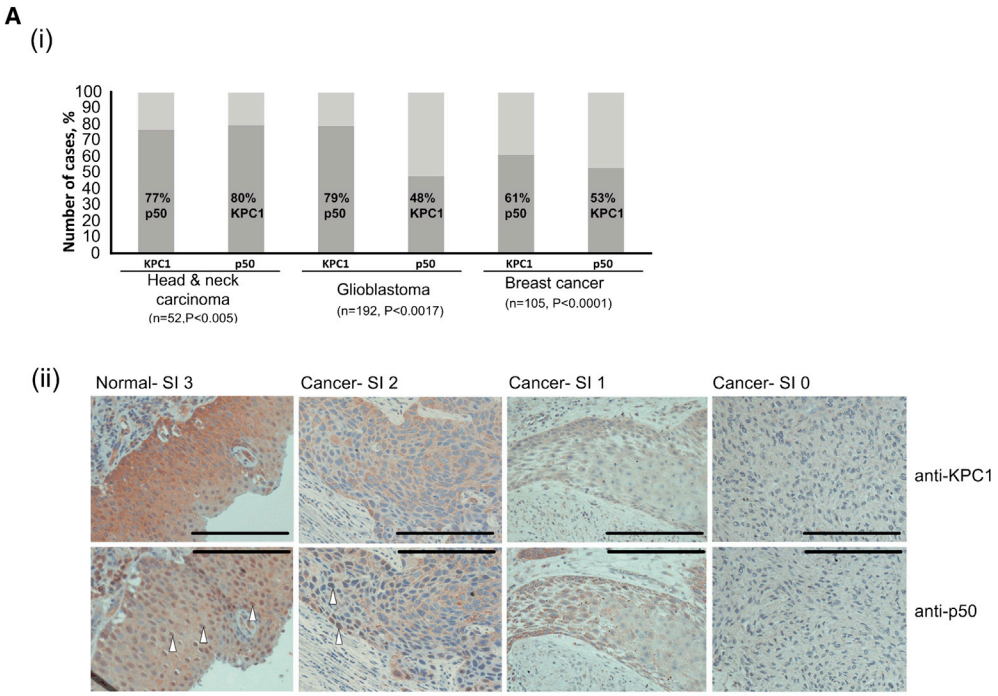

B

Tissue		Sample size	Average of KPC1 SI		KPC1 stained, %		Nuclear p50, %	
Head & neck	Normal	11	P<0.0001	2.6	P<0.012	100	P<0.0015	100
	Cancer	52		1.12		62		47
Glial cells	Normal	16	P<0.03	1.625	N.S.	100	P<0.0001	75
	Cancer	192		1.365		84		19.7
Breast	Normal	20	N.S.	1.37	N.S.	90	P<0.0001	65
	Cancer	85		1.25		94		17.6

Figure 7. Correlation between the Expression of KPC1 and p50 in Tumoral and Normal Human Tissues

(A) (i) Correlation between expression of KPC1 and p50 in tumors. Immunohistochemistry of KPC1 and p50 in serial sections from SCCHN, and glioblastoma and breast cancer tissue arrays. P, p value. Analyses were carried out as described in the Experimental Procedures. (ii) Representative immunostaining of SCCHN sections with anti-KPC1 or anti-p50. SI, staining intensity from 3 (strong positive) to 0 (negative). Arrowheads point to nuclear staining. Scale bars, 100 μm.

(B) Statistical analysis of p50 and KPC1 staining in normal and cancerous head and neck, glial and breast tissues. "Average of KPC1 SI" represents mean of sample staining (number of samples is indicated under "Sample size"). "KPC1 stained, %" and "nuclear p50, %" represent percent of samples stained for KPC1 or nuclear p50. P, p value. The p value reflects the significance of difference between staining of normal and cancer tissue. SI, staining intensity; N.S., non-significant.

See also Figure S6.

(high salt eluate) as described (Hershko et al., 1983). Fraction II (~200 mg) was further resolved using different successive chromatographic methods as described in the Extended Experimental Procedures.

In Vitro Translation

p105 or p100 were translated in vitro in the presence of L-[^{35}S]methionine using the TNT T7 Quick reticulocyte lysate-based coupled transcription-translation kit according to the manufacturer's instructions.

In Vitro Conjugation and Processing of p105

Ub conjugation and processing of ^{35}S-labeled p105 were carried out in a reconstituted cell-free system containing crude Fraction II as described (Kravtsova-Ivantsiv et al., 2009). For conjugation, 1 μg of purified Kpc1-FLAG-TEV-6xHIS, Kpc1I1256A-FLAG-TEV-6xHIS, or 6xHis-KPC2 were added as indicated instead of Fraction II.

Ub Conjugates in Cells

HEK293 cells were transfected with control siRNA or siRNA against KPC1 as described above. After 24 hr, the cells were transfected with cDNAs coding for FLAG-p105 proteins along with cDNAs coding for HA-Ub and Myc-KPC1, or with an empty vector. After additional 24 hr, the proteasome inhibitor MG132 (20 μM) was added for 3 hr, and the cells were lysed with RIPA buffer supplemented with freshly dissolved iodoacetamide and *N*-ethylmaleimide (5 mM each) to inhibit deubiquitinating enzymes. p105 (both free and

ubiquitinated) and free p50 were immunoprecipitated with immobilized anti-FLAG. The beads were washed five times with RIPA buffer and proteins were resolved by SDS-PAGE. Free and conjugated p105 (and free p50) were visualized using anti-FLAG.

Tumorigenicity

Cell-based (soft agar) and animal (mice xenografts) tumorigenicity assays are described in the Extended Experimental Procedures.

RNA-Seq Analysis

RNA from U87-MG xenografts was isolated using RNA purification kit and analyzed using the Illumina HiSeq 2500 analyzer. Identification and clustering of the human genes are described in the Extended Experimental Procedures.

Immunohistochemistry and Statistical Analysis

The staining technique and statistical analysis of the staining data of SCCHN, breast cancer, and glioblastoma were performed as described in the Extended Experimental Procedures.

ACCESSION NUMBERS

The profile of gene expression in the tumors using RNA-seq analysis of transcripts reported in this paper is deposited in NCBI GEO under accession number GSE60530 and is available at http://www.ncbi.nlm.nih.gov/geo/query/acc.cgi?acc=GSE60530.

SUPPLEMENTAL INFORMATION

Supplemental Information includes Extended Experimental Procedures, six figures, two tables, and one data file and can be found with this article at http://dx.doi.org/10.1016/j.cell.2015.03.001

AUTHOR CONTRIBUTIONS

A.C., T.S., and Y.T.K. contributed to the study design. Y.K.-I., I.S., and V.C.-K. contributed to the study design and carried out the biochemical and tumorigenicity assays. H.G. contributed to some of the biochemical experiments. T.Z. and A.A. performed the mass spectrometry analyses. I.N. and E.P. carried out the pathological observations. I.D. performed the statistical analyses of the stained human tumors. B.S. and G.S.-F. performed the computational analysis of the RNA-seq data. A.B. and M.J. synthetized the peptides and planned some of the experiments. A.C. supervised the study. Y.K.-I., I.S., and A.C. wrote the manuscript.

ACKNOWLEDGMENTS

Research in the laboratory of A.C. is supported by grants from the Dr. Miriam and Sheldon G. Adelson Medical Research Foundation (AMRF), the Israel Science Foundation (ISF), the I-CORE Program of the Planning and Budgeting Committee and the ISF (Grant1775/12), the EU Treat PolyQ Network, the Nobel Laureates Invitation Program of Seoul National University, the Deutsch-Israelische Projektkooperation (DIP), and the Program for Targeting Cancer by Modulating Protein Dynamics supported by Albert Sweet (Malibu, CA). We thank Dr. Kazuhiro Iwai (Department of Molecular and Cellular Physiology, Graduate School of Medicine, Kyoto University, Sakyo-ku, Kyoto, Japan) for providing us with some cDNAs. RNA-seq and mapping to the human genome was done by the Technion Genome Center. B.S. is supported by a fellowship from the Swiss National Science Foundation. Y.T.K. is supported by The Basic Science Research Programs of the National Research Foundation of Korea (NRF-2013R1A2A2A01014170). A.C. is an Israel Cancer Research Fund (ICRF) USA Professor.

Received: August 15, 2014
Revised: December 29, 2014
Accepted: February 25, 2015
Published: April 9, 2015

REFERENCES

Akiri, G., Cherian, M.M., Vijayakumar, S., Liu, G., Bafico, A., and Aaronson, S.A. (2009). Wnt pathway aberrations including autocrine Wnt activation occur at high frequency in human non-small-cell lung carcinoma. Oncogene *28*, 2163–2172.

Anders, S., Pyl, P.T., and Huber, W. (2015). HTSeq-a Python framework to work with high-throughput sequencing data. Bioinformatics *31*, 166–169.

Barré, B., and Perkins, N.D. (2007). A cell cycle regulatory network controlling NF-κB subunit activity and function. EMBO J. *26*, 4841–4855.

Barré, B., Coqueret, O., and Perkins, N.D. (2010). Regulation of activity and function of the p52 NF-κB subunit following DNA damage. Cell Cycle *9*, 4795–4804.

Ben-Neriah, Y., and Karin, M. (2011). Inflammation meets cancer, with NF-κB as the matchmaker. Nat. Immunol. *12*, 715–723.

Betts, J.C., and Nabel, G.J. (1996). Differential regulation of NF-κB2(p100) processing and control by amino-terminal sequences. Mol. Cell. Biol. *16*, 6363–6371.

Bonavia, R., Inda, M.M., Cavenee, W.K., and Furnari, F.B. (2011). Heterogeneity maintenance in glioblastoma: a social network. Cancer Res. *71*, 4055–4060.

Carette, J.E., Raaben, M., Wong, A.C., Herbert, A.S., Obernosterer, G., Mulherkar, N., Kuehne, A.I., Kranzusch, P.J., Griffin, A.M., Ruthel, G., et al. (2011). Ebola virus entry requires the cholesterol transporter Niemann-Pick C1. Nature *477*, 340–343.

Cohen, S., Achbert-Weiner, H., and Ciechanover, A. (2004). Dual effects of IκB kinase β-mediated phosphorylation on p105 Fate: $SCF^{(\beta\text{-}TrCP)}$-dependent degradation and $SCF^{(\beta\text{-}TrCP)}$-independent processing. Mol. Cell. Biol. *24*, 475–486.

Cohen, S., Lahav-Baratz, S., and Ciechanover, A. (2006). Two distinct ubiquitin-dependent mechanisms are involved in NF-κB p105 proteolysis. Biochem. Biophys. Res. Commun. *345*, 7–13.

Deng, W.G., and Wu, K.K. (2003). Regulation of inducible nitric oxide synthase expression by p300 and p50 acetylation. J. Immunol. *171*, 6581–6588.

Dennis, G., Jr., Sherman, B.T., Hosack, D.A., Yang, J., Gao, W., Lane, H.C., and Lempicki, R.A. (2003). DAVID: Database for Annotation, Visualization, and Integrated Discovery. Genome Biol. *4*, 3.

DiDonato, J.A., Mercurio, F., and Karin, M. (2012). NF-κB and the link between inflammation and cancer. Immunol. Rev. *246*, 379–400.

Fan, C.M., and Maniatis, T. (1991). Generation of p50 subunit of NF-κB by processing of p105 through an ATP-dependent pathway. Nature *354*, 395–398.

Fujita, T., Nolan, G.P., Liou, H.C., Scott, M.L., and Baltimore, D. (1993). The candidate proto-oncogene bcl-3 encodes a transcriptional coactivator that activates through NF-κB p50 homodimers. Genes Dev. *7*, 1354–1363.

Gao, J., Chen, T., Liu, J., Liu, W., Hu, G., Guo, X., Yin, B., Gong, Y., Zhao, J., Qiang, B., et al. (2009). Loss of NECL1, a novel tumor suppressor, can be restored in glioma by HDAC inhibitor-Trichostatin A through Sp1 binding site. Glia *57*, 989–999.

Hara, T., Kamura, T., Kotoshiba, S., Takahashi, H., Fujiwara, K., Onoyama, I., Shirakawa, M., Mizushima, N., and Nakayama, K.I. (2005). Role of the UBL-UBA protein KPC2 in degradation of p27 at G1 phase of the cell cycle. Mol. Cell. Biol. *25*, 9292–9303.

Heddleston, J.M., Li, Z., McLendon, R.E., Hjelmeland, A.B., and Rich, J.N. (2009). The hypoxic microenvironment maintains glioblastoma stem cells and promotes reprogramming towards a cancer stem cell phenotype. Cell Cycle *8*, 3274–3284.

Heissmeyer, V., Krappmann, D., Hatada, E.N., and Scheidereit, C. (2001). Shared pathways of IkappaB kinase-induced $SCF^{(\beta\text{-}TrCP)}$-mediated ubiquitination and degradation for the NF-κB precursor p105 and IκBalpha. Mol. Cell. Biol. *21*, 1024–1035.

Hershko, A., Heller, H., Elias, S., and Ciechanover, A. (1983). Components of ubiquitin-protein ligase system. Resolution, affinity purification, and role in protein breakdown. J. Biol. Chem. *258*, 8206–8214.

Ivanov, V.N., Lee, R.K., Podack, E.R., and Malek, T.R. (1997). Regulation of Fas-dependent activation-induced T cell apoptosis by cAMP signaling: a potential role for transcription factor NF-κB. Oncogene *14*, 2455–2464.

Kamura, T., Hara, T., Matsumoto, M., Ishida, N., Okumura, F., Hatakeyama, S., Yoshida, M., Nakayama, K., and Nakayama, K.I. (2004). Cytoplasmic ubiquitin ligase KPC regulates proteolysis of $p27^{Kip1}$ at G1 phase. Nat. Cell Biol. *6*, 1229–1235.

Kravtsova-Ivantsiv, Y., Cohen, S., and Ciechanover, A. (2009). Modification by single ubiquitin moieties rather than polyubiquitination is sufficient for proteasomal processing of the p105 NF-κB precursor. Mol. Cell *33*, 496–504.

Lin, L., and Ghosh, S. (1996). A glycine-rich region in NF-κB p105 functions as a processing signal for the generation of the p50 subunit. Mol. Cell. Biol. *16*, 2248–2254.

Lin, L., DeMartino, G.N., and Greene, W.C. (1998). Cotranslational biogenesis of NF-κB p50 by the 26S proteasome. Cell *92*, 819–828.

Love, M.I., Huber, W., and Anders, S. (2014). Moderated estimation of fold change and dispersion for RNA-seq data with DESeq2. Genome Biol. *15*, 550.

MacKichan, M.L., Logeat, F., and Israël, A. (1996). Phosphorylation of p105 PEST sequence via a redox-insensitive pathway up-regulates processing of p50 NF-κB. J. Biol. Chem. *271*, 6084–6091.

May, M.J., and Ghosh, S. (1997). Rel/NF-κB and IκB proteins: an overview. Semin. Cancer Biol. *8*, 63–73.

Mercer, J., Snijder, B., Sacher, R., Burkard, C., Bleck, C.K., Stahlberg, H., Pelkmans, L., and Helenius, A. (2012). RNAi screening reveals proteasome- and Cullin3-dependent stages in vaccinia virus infection. Cell Rep. *2*, 1036–1047.

Mercurio, F., Zhu, H., Murray, B.W., Shevchenko, A., Bennett, B.L., Li, J., Young, D.B., Barbosa, M., Mann, M., Manning, A., and Rao, A. (1997). IKK-1 and IKK-2: cytokine-activated IκB kinases essential for NF-κB activation. Science *278*, 860–866.

Niwa, H., Yamamura, K., and Miyazaki, J. (1991). Efficient selection for high-expression transfectants with a novel eukaryotic vector. Gene *108*, 193–199.

Orian, A., Gonen, H., Bercovich, B., Fajerman, I., Eytan, E., Israël, A., Mercurio, F., Iwai, K., Schwartz, A.L., and Ciechanover, A. (2000). $SCF^{(\beta\text{-}TrCP)}$ ubiquitin ligase-mediated processing of NF-κB p105 requires phosphorylation of its C-terminus by IκB kinase. EMBO J. *19*, 2580–2591.

Palombella, V.J., Rando, O.J., Goldberg, A.L., and Maniatis, T. (1994). The ubiquitin-proteasome pathway is required for processing the NF-κB1 precursor protein and the activation of NF-κB. Cell *78*, 773–785.

Perkins, N.D. (2012). The diverse and complex roles of NF-κB subunits in cancer. Nat. Rev. Cancer *12*, 121–132.

Perrella, M.A., Pellacani, A., Wiesel, P., Chin, M.T., Foster, L.C., Ibanez, M., Hsieh, C.M., Reeves, R., Yet, S.F., and Lee, M.E. (1999). High mobility group-I(Y) protein facilitates NF-κB binding and transactivation of the inducible nitric-oxide synthase promoter/enhancer. J. Biol. Chem. *274*, 9045–9052.

Pikarsky, E., and Ben-Neriah, Y. (2006). NF-κB inhibition: a double-edged sword in cancer? Eur. J. Cancer *42*, 779–784.

Rahman, M.M., and McFadden, G. (2011). Modulation of NF-κB signalling by microbial pathogens. Nat. Rev. Microbiol. *9*, 291–306.

Salmerón, A., Janzen, J., Soneji, Y., Bump, N., Kamens, J., Allen, H., and Ley, S.C. (2001). Direct phosphorylation of NF-κB1 p105 by the IκB kinase complex on serine 927 is essential for signal-induced p105 proteolysis. J. Biol. Chem. *276*, 22215–22222.

Senftleben, U., Cao, Y., Xiao, G., Greten, F.R., Krahn, G., Bonizzi, G., Chen, Y., Hu, Y., Fong, A., Sun, S.C., and Karin, M. (2001). Activation by IKKa of a second, evolutionary conserved, NF-κB signaling pathway. Science *293*, 1495–1499.

Siggers, T., Chang, A.B., Teixeira, A., Wong, D., Williams, K.J., Ahmed, B., Ragoussis, J., Udalova, I.A., Smale, S.T., and Bulyk, M.L. (2012). Principles of dimer-specific gene regulation revealed by a comprehensive characterization of NF-κB family DNA binding. Nat. Immunol. *13*, 95–102.

Szklarczyk, D., Franceschini, A., Kuhn, M., Simonovic, M., Roth, A., Minguez, P., Doerks, T., Stark, M., Muller, J., Bork, P., et al. (2011). The STRING database in 2011: functional interaction networks of proteins, globally integrated and scored. Nucleic Acids Res. *39*, D561–D568.

Trapnell, C., Pachter, L., and Salzberg, S.L. (2009). TopHat: discovering splice junctions with RNA-Seq. Bioinformatics *25*, 1105–1111.

UniProt Consortium (2013). Update on activities at the Universal Protein Resource (UniProt) in 2013. Nucleic Acid Res. *41*, D43–D47.

Voce, D.J., Schmitt, A.M., Uppal, A., McNerney, M.E., Bernal, G.M., Cahill, K.E., Wahlstrom, J.S., Nassiri, A., Yu, X., Crawley, C.D., et al. (2014). NF-κB1 is a haploinsufficient DNA damage-specific tumor suppressor. Oncogene. http://dx.doi.org/10.1038/onc.2014.211.

Zaaroor-Regev, D., de Bie, P., Scheffner, M., Noy, T., Shemer, R., Heled, M., Stein, I., Pikarsky, E., and Ciechanover, A. (2010). Regulation of the polycomb protein Ring1B by self-ubiquitination or by E6-AP may have implications to the pathogenesis of Angelman syndrome. Proc. Natl. Acad. Sci. USA *107*, 6788–6793.

Zhao, M., Sun, J., and Zhao, Z. (2013). TSGene: a web resource for tumor suppressor genes. Nucleic Acids Res. *41*, D970–D976.

EXTENDED EXPERIMENTAL PROCEDURES

Materials

Materials for SDS-PAGE and Bradford reagent were from Bio-Rad. L-[^{35}S]methionine and pre-stained MW markers were from GE Healthcare. Tissue culture sera, media, and supplements, were from Sigma or from Biological Industries [Bet HaEmek, Israel; except for the FCS used for growing Sf9 cells that was from Hyclone, and Iscove's Modified Dulbecco's Medium (IMDM) for growing HAP1 cells that was from GIBCO]. HAP1 control cells (Carette et al., 2011) and HAP1 cells knocked out for KPC1 [1bp insertion (nucleotide is underlined and bolded) in exon 4 (NM_022064; 192-CCAGAACATTTGGACCAGTT**G**GCTACAGGTGGACAATGAGG-232; the insertion results in a frameshift] or KPC2 [1bp insertion (nucleotide is underlined and bolded) in exon 2 (NM_016172; 210-GTGCTGAGT GATGCCAGGAC**A**CATCCTGGAAGAGAACATCC-250; the insertion results in a frameshift] were generated by Haplogen Genomics GmbH (Vienna, Austria), using the Crispr-CAS technology. Collagenase I was from Sigma and Dispase II from Roche. Free and immobilized mouse anti-FLAG (M2), rabbit anti-p50 Prestige Antibodies (for immunoprecipitation and western blot), and FLAG peptide, were from Sigma. Mouse anti-HA (16B12) was from Covance, and rabbit anti-p50 (NLS) and its blocking peptide, mouse anti-KPC1 (267.1 for western blot), anti-p65 (A), anti-p27 (C-19) and anti-GFAP (H-50), were from Santa Cruz. Anti-KPC1 (ab57549 for immunohistochemistry and for western blot) was from Abcam, whereas anti-cleaved caspase 3 (D175) was from Cell Signaling. Anti-ki-67 (MIB-1) was from DAKO, and anti-actin was from Millipore. Peroxidase-conjugated (for western blotting) and Rhodamine Red-X-conjugated goat anti-rabbit (for immunofluorescence) secondary antibody were from Jackson ImmunoResearch Laboratories. VECTASHIELD Mounting Medium with DAPI was from Vector Laboratories. Secondary HRP-conjugated antibody HISTOFINE Simple Stain, Max Po Universal Immuno Peroxidase Polymer anti-rabbit/anti-mouse, and HISTOFINE Simple Stain AEC solution for immunohistochemistry, were from Nichirei Biosciences. Ubiquitin, dithiothreitol (DTT), phosphocreatine, creatine phosphokinase, adenosine 5′-triphosphate (ATP), adenosine 5′-[γ-thiotriphosphate] (ATPγS), iodoacetamide, *N*-ethylmaleimide, Tris and HEPES buffers, paraformaldehyde, crystal violet, and O-nitrophenyl-beta-D-galactopyranoside (ONPG), were from Sigma. Protease inhibitors mixture and N-carbobenzoxy-L-leucyl-L-leucyl-leucinal (MG132) were from Calbiochem. Ub aldehyde (UbAl) was from BIOMOL. Reagents for enhanced chemiluminescence (ECL) were from Pierce. TNT T7 Quick reticulocyte lysate-based coupled transcription/translation kit and the luciferase reporter 1000 assay system were from Promega. JetPEI cell transfection reagent was from Polyplus. Lipofectamine RNAiMAX and Lipofectamine 2000 transfection reagents for siRNA and for DNA transfection, respectively, and Bac-to-Bac baculovirus expression system, were from Invitrogene. siRNAs were synthesized by Dharmacon. shRNAs, RevertAid H Minus First Strand cDNA Synthesis Kit, Shandon Immune-Mount, and LightShift Chemiluminescent ElectroMobility Shift Assay (EMSA) kit, were from Thermo Scientific. TaqMan Fast Universal PCR Master Mix and TaqMan Gene Expression Assay were from Applied Biosystems. Restriction and modifying enzymes were from New England Biolabs. Oligonucleotides were synthesized by Syntezza Bioscience or by Sigma. All the chromatographic columns were purchased from GE Healthcare except for the hydroxyapatite column that was from BioRad. Low Melt Agarose and mini-PROTEAN TBE precast gel (5%, for separation of dsDNA) were from Bio-Rad. DEAE cellulose was purchased from Whatman. Ni-NTA resin was from QIAGEN. Glioblastoma and breast tissue microarrays were from US Biomax. NucleoSpin Kit for RNA purification was from Macherey-Nagel. All other reagents were of high analytical grade.

Plasmid Construction

cDNAs coding for human p105 and p105S927A for in vitro translation (in pT7β-6xHIS) and transient transfection in cells (in pFLAG-CMV2), were described previously (Cohen et al., 2004, 2006). For in vitro translation of deleted species of p105 (p105Δ500-600, p105Δ565-660, p105Δ647-758, p105Δ752-794, p105Δ544-803), the corresponding cDNAs were generated by PCR and cloned into the pT7β-6xHIS BamHI and EcoRI restriction sites. For transient transfection of the deleted species of p105 in cells, the cDNA fragments with the deletions that were cloned initially into pT7β-6xHIS, were sub-cloned into the PstI restriction site in pFLAG-CMV2p105 or pFLAG-CMV2p105S927A. FLAG-p105K594,625,630,637,639,640,684,740R (FLAG-p105K8R; where all the lysine residues in the ankyrin repeats and in between them were substituted with arginines) in pFLAG-CMV2, was generated by site-directed mutagenesis. FLAG-p105Δ574-803 (in which all but one of the ankyrin repeats were deleted) was generated by PCR and was cloned into the pFLAG-CMV2 NotI restriction site. cDNA coding for p100 was amplified with primers flanked with HindIII and BamHI restriction sites, and was cloned into pFLAG-CMV2.

cDNAs coding for human p105K46-58R, p105Δ429-654, and p105Δ429-654;K29,K46-58R for in vitro translation (in pT7β-6xHIS), and p105Δ429-654 and p105Δ429-654;K29,K46-58R for transient transfection (in pFLAG-CMV2), were described previously (Cohen et al., 2004, 2006). The cDNA coding for p105K46-58R was amplified (using pT7βp105K46-58R as a template) with primers flanked with NotI restriction site, and was cloned into pFLAG-CMV2.

cDNAs coding for HA-Ub, Myc-KPC1, and Myc-KPC1I1256A for expression in mammalian cells sub-cloned into pCAGGS (Niwa et al., 1991), were kindly provided by Dr. Kazuhiro Iwai.

KPC1-FLAG-TEV-6xHIS and KPC1I1256A-FLAG-TEV-6xHIS for expression in insect cells were cloned into pFastBac via several steps. Initially, the N-terminal segment of KPC1 was amplified with primers flanked with BsshII and EcoRI, and the C-terminal segment of KPC1 was amplified with primers flanked with EcoRI and SalI. The two fragments were sub-cloned into the appropriate restriction sites of pFastBac. Finally, FLAG-TEV-6xHIS was introduced into pFastBac using the SalI restriction site.

cDNA coding for KPC2 for expression in bacterial cells was amplified with primers flanked with EcoRI and HindIII restriction sites, and was sub-cloned into pT7β-6xHIS.

cDNAs coding for FLAG-IKKβ and the constitutively active FLAG-IKKβS176,180E were as described (Mercurio et al., 1997).

cDNA coding for NIK was as described (Senftleben et al., 2001).

cDNA coding for 6xHIS-E6-AP was as described (Zaaroor-Regev et al., 2010).

cDNAs coding for Myc-KPC1, Myc-KPC1I1256A, and FLAG-p50 for generation of cells that stably express these proteins, were amplified with primers flanked with XhoI and BamHI or with XhoI, respectively, and were sub-cloned into the NSPI-CMV MCS lentiviral expression vector (Akiri et al., 2009).

cDNA coding for p65 was amplified with primers flanked with BamHI and was sub-cloned into pT7β-6xHIS BamHI restriction site.

Cultured Cells

HEK293, HeLa, U2OS, MDA-MB 231 and U87-MG were grown at 37°C in DMEM supplemented with 10% fetal calf serum and antibiotics (penicillin–streptomycin). Sf9 cells were grown in Grace's medium supplemented with 10% FCS, penicillin (100U/ml)/streptomycin (0.1 mg/ml), and yeastolate and lactalbumin (3.332 gr/l each). HAP1 cells were grown in IMDM supplemented with 10% fetal calf serum and antibiotics (penicillin–streptomycin).

Synthesis of p105-Derived Peptides

Synthetic phosphorylated and non-phosphorylated peptides derived from the p105 IKKβ-phosphorylation site (917-DELRD SDSVCD**S(P)**GVET**S(P)**FRKLSFTES-942) were prepared according to Fmoc-solid phase peptide synthesis strategy using HCTU (1-[Bis(dimethylamino)methylen]-5-chlorobenzotriazolium 3-oxide hexafluorophosphate, *N*,*N*,*N*′,*N*′-Tetramethyl-*O*-(6-chloro-1*H*-benzotriazol-1-yl)uronium hexafluorophosphate) and DIEA (*N*-Diisopropylethylamine) as coupling reagents. The synthesis was carried out on a Rink Amide resin using automated peptides synthesizer (CSBIO). Phosophorylated Ser was coupled as Fmoc-Ser(HPO3Bzl)OH. Cleavage of the peptide was performed using a mixture of 85:5:5:2.5:2.5 of TFA:water:thioanisole:phenol:ethanedithiol for 2 hr at room temperature. The peptide was precipitated using cold ether, dissolved in 50% acetonitile in water in the presence of 0.1% TFA. Purification was carried using preparative column (Jupiter 10 micron, C18/C4 300 Å, 250 × 22.4 mm) and a linear gradient of 5%–50% buffer containing 99.9% acetonitrile and 0.1% TFA over 30 min and with a flow rate of 15 ml/min. Fractions were analyzed by mass spectrometry using LCQ Fleet Ion Trap instrument (Thermo Scientific), and the fractions which showed over 85% purity were collected and lyophilized for use in the inhibition assay.

Fractionation of Crude Reticulocyte Lysate

Fraction II (~200 mg) was resolved on a HiLoad 16/10 Q Sepharose HP column using a linear salt gradient of 0.0–0.6 M KCl. Fractions that contained p105 Ub-conjugating activity were further resolved on a HiPrep Heparin 16/10 FF column, and proteins were eluted using a linear salt gradient of 0.0–1.0 M NaCl. The fractions with the p105 E3 activity were subjected to hydroxyapatite chromatography. Proteins were eluted using a linear gradient of 10–700 mM KPi pH 7.0. The active fractions were applied to a Mono Q 5/50 GL column, and proteins eluted using a linear salt gradient of 0.0–0.6 M KCl. The active fractions were resolved on a gel filtration HiLoad 16/600 Superdex 200 column. Elution was carried out in a buffer containing 20 mM Tris-HCl, pH 7.2, 150 mM NaCl, and 1 mM DTT. The E3 activity was eluted in a peak corresponding to an apparent native molecular size of ~170–300 kDa, and was applied to a HiTrap Heparin HP column. Elution was performed with a linear salt gradient of 0.0–1.0 M NaCl. The active fractions from the last three chromatographic steps were analyzed by mass spectrometry as described below.

Mass Spectrometric Analysis

Samples were digested by trypsin, analyzed by LC-MS/MS on Orbitrap XL (Thermo), and identified by Protein Discoverer software version 1.4 against the rabbit and mouse sections of the Uniprot database. The analysis was done using the Sequest search engine. The data were filtered with 1% FDR and 5 ppm accuracy.

Transient Transfection and Processing of p105 in Cells

HeLa cells were transiently transfected with the various indicated cDNAs using Lipofectamine 2000 according to the manufacturer's protocol, and HEK293 cells were transiently transfected using the jetPEI reagent. 24 hr after transfection, cycloheximide (20 μg/ml) was added for the indicated times, and the cells were harvested and lysed with RIPA buffer [150 mM NaCl, 0.5% sodium deoxycholate, 50 mM Tris-HCl (pH 8.0), 0.1% SDS, and 1% NP-40, supplemented with freshly added protease inhibitors mixture]. Protein aliquots representing an equal number of cells were resolved via SDS-PAGE (10%) and blotted onto nitrocellulose membrane. p105 or its mutant species were visualized using anti-FLAG, and processing was expressed as the ratio between the band density of p50 and the sum of the band densities of p105 and p50, multiplied by 100%, except when indicated otherwise. Actin was used as a loading control and was detected using a specific antibody.

Stable Transfection

For stable transfection, U87-MG, U2OS, and MDA-MB 231 cells were transfected with an empty vector, Myc-KPC1, Myc-KPC1I1256A, FLAG-p50, or with shRNA against p105 (clones IDs V2LHS_201580, V2LHS_201509, and V2LHS_201757) along with Myc-KPC1. Transfection was carried out using a Lentiviral transduction system, and cells were selected using puromycin (5 μg/ml).

siRNA

To silence human KPC1 and KPC2, we used the ON-TARGETplus SMART pool siRNAs synthesized by Dharmacon (for KPC1 -GCGCUACUAUUGGGAUGAA, CAACUGGGCCUUCUCUGAA, GCACAUGGCGGACCUCCUA, GGUGAAGCUUCUAGGUAUA; for KPC2 - GCUAAUUGAACACGCAGAA, GCACGUAGGUGGCGUUGUU, CAGAAUGCCGCGUGCGAGU, AGAGAUGAGCUGACG GAAA). Transfection of HEK293 cells with the siRNA oligonucleotides was performed using Lipofectamine RNAiMAX according to the manufacturer's instructions. Briefly, HEK293 cells were grown to 85% confluence in a medium that was not supplemented with antibiotics. KPC1 or KPC2 siRNAs (40 nM) were added to the medium. The efficiency of gene expression suppression was monitored 48 hr after transfection by western blot using anti-KPC1 or anti-KPC2.

Protein-Protein Interactions

For analyses of protein-protein interactions, HEK293 cells were transfected with cDNAs coding for FLAG-p105 proteins along with cDNA coding for Myc-KPC1 or with an empty vector. p105 proteins were immunoprecipitated with immobilized anti-FLAG, and following washing of the beads with RIPA buffer, the immunoprecipitated proteins were resolved by SDS-PAGE. p105, p50 and KPC1 were visualized using anti-FLAG or anti-KPC1. For interaction between endogenous proteins, HeLa cells were lysed with RIPA buffer, and p105 was immunoprecipitated with anti-p50. Following washing of the beads with RIPA buffer, the immunoprecipitated proteins were resolved by SDS-PAGE. p105, p50 and KPC1 were visualized using anti-p50 or anti-KPC1.

Protein Expression Using a Baculovirus Expression System

KPC1-FLAG-TEV-6xHIS and KPC1I1256A-FLAG-TEV-6xHIS were cloned into pFastBac vector as described above. Recombinant Baculovirus constructs were generated using Bac-to-Bac expression system. To express the proteins, Sf9 cells were infected with the generated viruses. After 48 hr, cells were harvested and lysed in a buffer that contained 50 mM sodium phosphate buffer (pH 8.0), 600 mM NaCl, 10 mM imidazole, 1% NP40, and protease inhibitor cocktail (EDTA free).

Protein Expression Using a Bacterial Expression System

6xHIS-Ubc5c and 6xHIS-KPC2 were transformed to Rosetta (DE3) pLysS *Escherichia coli* cells (Novagen). The bacteria were grown to 0.7 OD at 37°C, and protein expression was induced with IPTG (0.5 mM). After 4 hr, cells were harvested and lysed by sonication in a buffer that contained 20 mM Tris-HCl (pH 7.6), 100 mM NaCl, 10 mM β-mercaptoethanol, and protease inhibitor cocktail (EDTA free). 6xHIS-E6-AP was expressed as described (Zaaroor-Regev et al., 2010).

Protein Purification

HIS-tagged proteins were purified under native conditions using Ni-NTA resin according to the manufacturer's instructions.

Colony Formation in Soft Agar

3 ml of DMEM containing 0.5% Low Melt Agarose and 10% fetal calf serum were poured into a 60 mm Petri dish. The layer was covered with 0.7×10^4 cells suspended in 1.5 ml DMEM that contains 0.3% Low Melt Agarose and 10% fetal calf serum, followed by addition of 2 ml DMEM containing 10% fetal calf serum. Medium was changed every 3 days. After three weeks, colonies were fixed (using 4% PFA), stained (with crystal violet; 0.05%), and counted, using the OpenCFU software for colony counting (http://opencfu.sourceforge.net).

Tumorigenicity

Exponentially growing U87-MG or MDA-MB 231 cells were stably transfected with an empty vector (V0) or with vectors coding for Myc-KPC1, Myc-KPC1I1256A or FLAG-p50. Cells were dissociated with trypsin, washed with PBS, and brought to a concentration of 50×10^6 cells/ml. Cell suspension (5×10^6/0.1 ml) was inoculated subcutaneously at the right flank of 7-weeks old Balb/C nude mice (n = 7). Xenograft size was determined twice a week by externally measuring the growing tumors in two dimensions using a caliper. Tumor volume (V) was determined by the equation $V = L \times W^2 \times 0.5$, where L is the length and W the width of the xenograft. At the end of the experiment, mice were sacrificed and xenografts were resected, weighed and fixed in formalin. Paraffin-embedded 5 μm sections were stained with antibodies as described above. All animal experiments were approved by the accredited Animal Care Committee of the Technion in Haifa, Israel.

Immunohistochemistry

Formalin-fixed, paraffin-embedded, 5 μm tissue sections of SCCHN, mice U87-MG xenografts, and glioblastoma and breast cancer tissue microarrays, or HEK293 cultured cells, were immunostained for p50, KPC1, ki-67, cleaved caspase 3, anti-p27 and GFAP, as indicated. Immunostaining was performed as following: slides were de-paraffinized and rehydrated, and endogenous peroxidase activity was quenched (for 30 min) by 3% hydrogen peroxide in methanol. Slides were then subjected to antigen retrieval by boiling (for 20 min) in 10 mM citrate buffer, pH 6.0. Slides were incubated with 10% normal goat serum in PBS for 60 min to block nonspecific binding, and were incubated (for 20 hr at 4°C) with the specific antibody (5 μg/ml) in blocking solution. Slides were then extensively washed with PBS, incubated with a secondary HRP-conjugated antibody for 60 min, and developed using AEC solution for 5 min

according to the manufacturer's instructions. Sections were stained with hematoxylin or hematoxylin and eosin, and mounted using the Shandon Immune-Mount.

Immunofluorescence Staining

U87-MG cells ($5x10^5$) were grown on coverslips for 2 days, washed three times with PBS, and fixed/permeabilized in paraformaldehyde (4% for 20 min at room temperature), followed by incubation in Triton X-100 (0.5% for 1min). The coverslips were washed three times with PBS, incubated with 10% normal goat serum in PBS for 60 min (to block nonspecific binding), and were incubated (for 24 hr at 4°C) with the specific antibody (5 μg/ml) in blocking solution. Following extensive washing with PBS, the coverslips were incubated with an appropriate secondary antibody (7 μg/ml) for 60 min, followed by three washes with PBS. They were then stained with 4'-6'-diamidino-2-phenylindole (DAPI) in mounting medium. Staining was examined using confocal microscope.

Electrophoretic Mobility Shift Assay

Extracts from U87-MG xenografts were isolated using tissue homogenizer in lysis buffer containing 20 mM HEPES (pH 8.0), 400 mM NaCl, 1 mM EDTA (pH 8.0), 1.5 mM $MgCl_2$, 1 mM DTT and 0.05% NP-40. For studying DNA-protein interaction, we used the LightShift Chemiluminescent EMSA kit according to the manufacturer's instructions. Briefly, extract (5 μg of protein) was incubated with duplex biotin end-labeled oligonucleotide representing the consensus NF-κB binding site [5′-AGTTGA**GGGGACTTTCCC**AGGC-biotin-3′ (bolded and underlined nucleotides denotes NF-κB binding consensus)], subjected to gel electrophoresis on a native polyacrylamide gel (5%), and transferred to a nylon membrane. The biotin end-labeled DNA was detected using the Streptavidin-Horseradish peroxidase conjugate and a chemiluminescent substrate.

Quantitative Real-Time PCR

RNA from U87-MG xenografts was isolated using an RNA purification kit and converted to cDNA using cDNA Synthesis Kit. The quantitative real-time PCR (qRT-PCR) was carried out using TaqMan Gene Expression Assay. The assay was carried out in triplicates using TaqMan primers for VCAM1, HIC1, CDKN2C, IL-6 and TES genes. HPRT gene was used as a control.

RNA-Seq Analysis Mapped to the Human Genome

RNA from U87-MG xenografts was isolated using an RNA purification kit, and analyzed using Illumina HiSeq 2500. The number of reads was between 25,949,993 and 39,809,768 per sample. The reads were mapped to the human genome (GRCh37) using Tophat version 2.0.9 (Trapnell et al., 2009). Up to 3 mismatches were allowed per read, with up to 3 mismatches per segment. The-b2-sensitive parameter was set. The unmapped reads were mapped later to the mouse genome as described below. The RNA-seq analysis experiment was repeated twice independently for KPC1 and V0 (in each experiment, RNA was pooled from tumors derived from different animals, and different pools were analyzed in duplicate or triplicate) and once for p50 (in duplicate of independent pools). Several repeated attempts to extract RNA from the p50-expressing tumors did not yield any results, as the tumors were miniscule.

Only uniquely mapped reads were counted in the analysis, using the HTSeq-count package version 0.5.3p3 with 'intersection-nonempty' mode (Anders et al., 2015).

The counts normalization and the differential expression analysis were done using the DESeq2 package version 1.2.8 (Love et al., 2014).

Computational Methods for Analyses of RNA-Seq Results

Bonferroni adjusted p values were calculated for the differentially expressed genes, and adjusted p values < 0.05 were considered as significant.

We looked for consistently up- or downregulated genes in the KPC1 and p50 overexpressing tumors, and selected only those that had a log2 fold change compared to empty-vector control of 0.7 or higher, or −0.7 or lower, respectively. Correlation was calculated as the Pearson linear correlation coefficient.

DAVID (Dennis et al., 2003) was used to perform functional enrichment analysis, using the functional annotation clustering tool and default settings on either the 534 up- or 48 downregulated genes. Annotation clusters were described with selected (most descriptive) annotations, and top selected annotation clusters are presented in Figure 6Aiii.

Tumor suppressor and proto-oncogene annotations were gathered from the TSGene database (Zhao et al., 2013) and UniProt (UniProt Consortium, 2013). All gene mappings between datasets were based on Ensembl Gene IDs, and significance of enrichment was calculated using the cumulative hyper geometric probability distribution function which takes into account the total number of genes measured, the number of cancer-related genes, the number of genes significantly up- or downregulated, and the overlap between those subsets.

Data for Integrative analysis of functional annotation clusters and known functional and physical protein-protein interactions between all consistently up- and downregulated genes (including NF-κB/p50 and KPC1; Figure 6C), were obtained from the STRING database (Szklarczyk et al., 2011). They were combined with interactions between genes and their most enriched annotation cluster from a DAVID analysis on the complete dataset. Details and source code of this integrative network method are provided elsewhere (Mercer et al., 2012).

Statistical Analysis of Staining of Cancerous and Normal Tissues for KPC1 and p50

The study included 52 patients with SCCHN who were diagnosed in the Department of Otolaryngology, Head and Neck Surgery, Carmel Medical Center, Haifa, Israel. The study protocol was approved by the local Institutional Review Board. Archival paraffin-embedded pathological material and surrounding normal tissue was obtained for immunohistochemical staining of KPC1 and p50. Breast cancer tissue arrays contained 85 malignant and 20 non-malignant slices. Glioblastoma tissue array contained 192 samples of glioblastoma and 16 normal brain tissue samples. Specimens were examined by a senior pathologist (I.N.) and were scored according to the intensity of staining (0: none, 1: weak; 2: moderate, 3: strong), and localization (cytoplasm versus nucleus).

The results were evaluated for normality using the Kolmogorov-Smirnov test. Correlations between variables were performed using the Pearson's or the Spearman's coefficients of correlation, for parametric or non-parametric groups, respectively. Matched analysis was done to compare staining of the normal tissue to the malignant one.

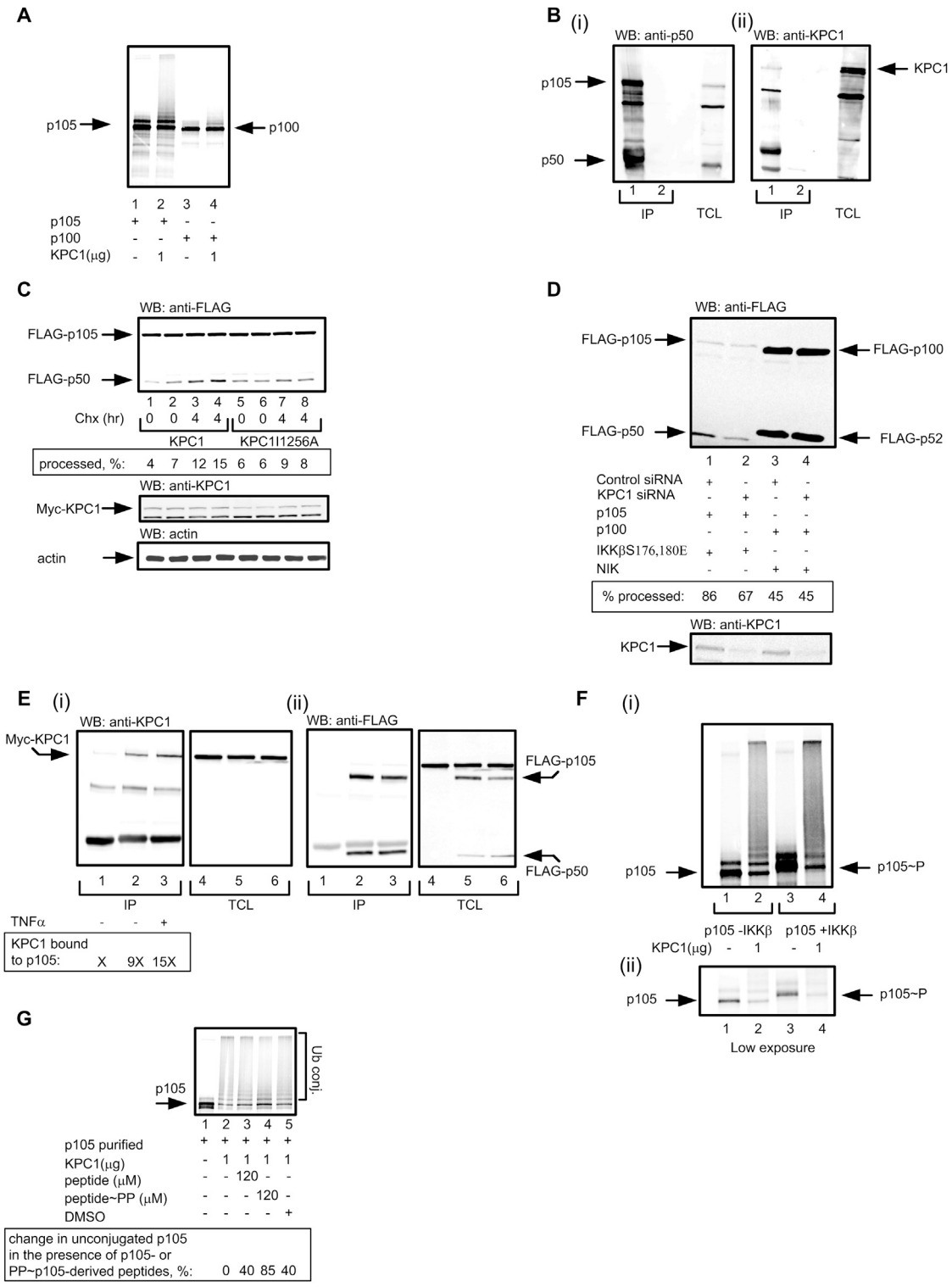

Figure S1. p105 Is a Substrate of KPC1 and KPC2 Ligase Complex, Related to Figure 2

(A) Ubiquitination of in vitro translated and ^{35}S-labeled p105 and p100 by purified KPC1-FLAG-TEV-6xHIS in a reconstituted cell free system.

(B) Co-immunoprecipitation of endogenous p105 and KPC1. Endogenous p105 was immunoprecipitated from HeLa cell lysate using anti-p50 (lane 1) or Protein G-immobilized beads (lane 2). Proteins were resolved via SDS-PAGE, blotted onto nitrocellulose membrane, and p105 and p50 were detected using anti-p50 (Panel i), and KPC1 was detected using anti-KPC1 (Panel ii). An aliquot (10%) of the total cell lysate (TCL) was analyzed for expression of the proteins.

(legend continued on next page)

(C) Cells expressing KPC1 RING domain-mutant process p105 less efficiently compared to those expressing WT KPC1. HEK293 cells were transfected with cDNAs coding for FLAG-p105 along with Myc-KPC1 or Myc-KPC1I1256A. 24 hr after transfection, cycloheximide was added for the indicated times, and cells were lysed, resolved via SDS-PAGE, and proteins visualized using anti-FLAG, anti-KPC1 or anti-actin as described under *Experimental Procedure*s. Chx denotes cyclohexamide. Actin was used to ascertain equal protein loading. Processing was assessed as described under Figure 2E.

(D) Silencing of KPC1 inhibits specifically signal-induced processing of p105 but not of p100. HEK293 cells were transfected with control siRNA (lanes 1, 3) or siRNA that targets KPC1 (lanes 2, 4). After 24 hr, cells were transfected with cDNAs coding for FLAG-p105, FLAG-p100, IKKβS176,180E or NIK, as indicated. After additional 24 hr, cells were lysed, resolved via SDS-PAGE, and proteins were visualized using anti-FLAG and anti-KPC1 as described under *Experimental Procedure*s. Processing was assessed as described under Figure 2E.

(E) The interaction between p105 and KPC1 is stimulated by TNFα. HeLa cells were transfected with cDNAs coding for FLAG-p105 (lanes 2 and 3) along with Myc-KPC1 (lanes 1-3). After 24 hr, cells were treated with TNFα (50 ng/ml) for 30 min (lane 3). FLAG-p105 was immunoprecipitated from the cell lysate using immobilized anti-FLAG (IP; lanes 1-3), and the bound KPC1 was visualized using anti-KPC1 (Ei; IP). p105 was visualized using anti-FLAG (Eii; IP). 10% of the total cell lysates (TCL; lanes 4-6) were analyzed for the expression of Myc-KPC1 or FLAG-p105 using anti-KPC1 (Ei) or anti-FLAG (Eii), respectively.

(F) Phosphorylation of p105 enhances its ubiquitination by KPC1. (i) Ubiquitination of in vitro translated and ^{35}S-labeled p105 or P∼p105 (phosphorylated by IKKβS176,180E; 1 μg added 20 min prior to the addition of the ligase; ATP, creatine phosphate and creatine phosphokinase were present in concentration of 0.1 mM, 10 mM, and 0.5 μg, respectively) was carried out by KPC1-FLAG-TEV-6xHIS in a reconstituted cell free system. (ii) The non-phosphorylated and phosphorylated forms of p105.

(G) A phosphorylated peptide corresponding to the signaled sequence in p105 inhibits ubiquitination of purified p105. In vitro translated and ^{35}S-labeled FLAG-p105 (immunoprecipitated by FLAG-beads, washed and released by the FLAG peptide; 100 μg/ml) was ubiquitinated by purified KPC1-FLAG-TEV-6xHIS (lanes 2-5) in a reconstituted cell free system in the presence of non-phosphorylated (lane 3) or phosphorylated (lane 4) peptides derived from the signaled sequence of p105. Presented is the change (in %) of free unconjugated p105 remained following addition of the peptides (compared to a system to which a peptide was not added; lane 2).

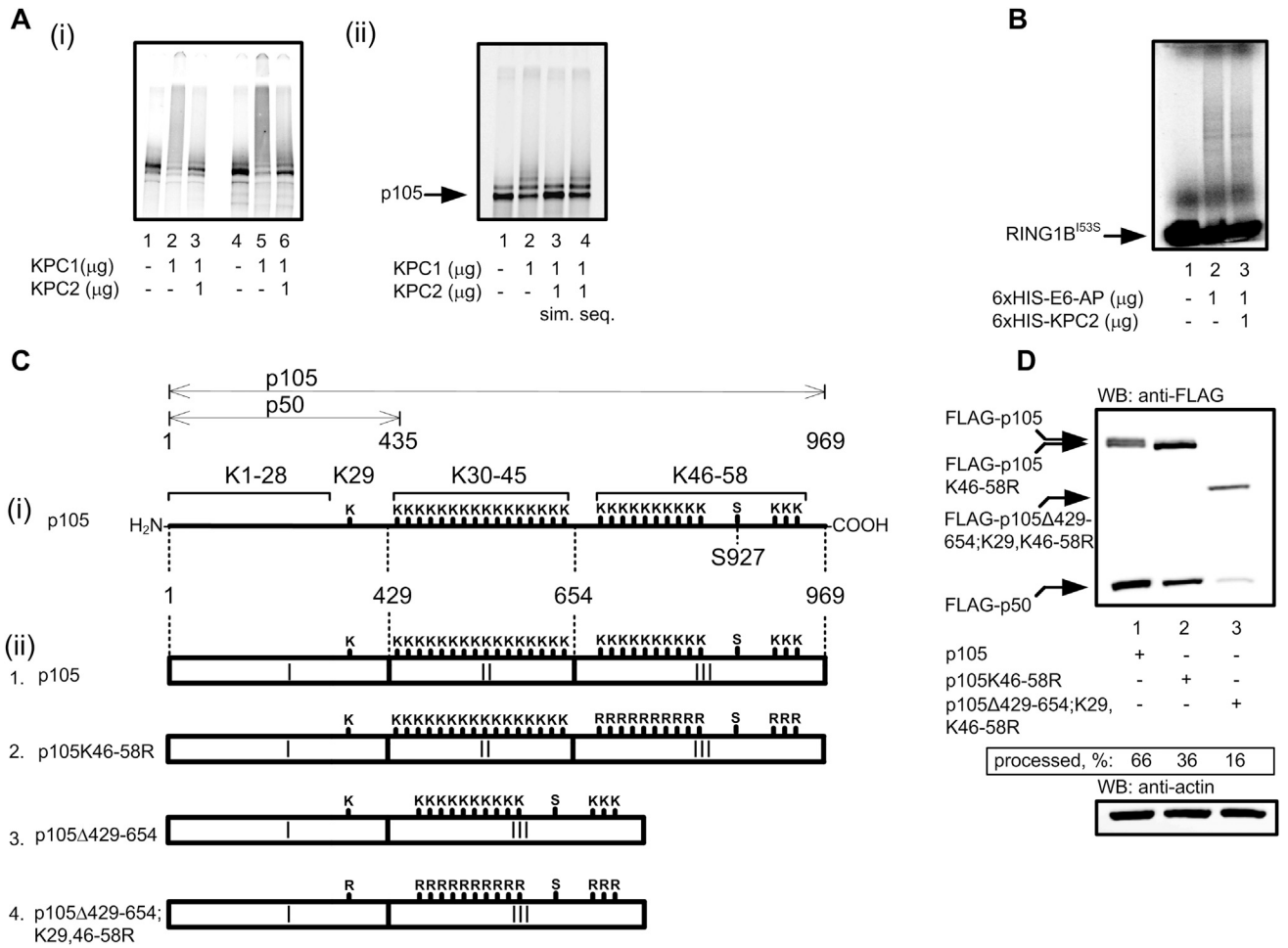

Figure S2. KPC2 Attenuates KPC1-Mediated Ubiquitination of p105 that Occurs on Lysine Residues in the C-Terminal Segment of the Precursor, Related to Figure 2

(A) Purified KPC1 ubiquitinates purified p105, a modification that is attenuated by purified KPC2 (lanes 1-3). (i) ^{35}S-labeled and in vitro translated FLAG-p105 was immunoprecipitated using FLAG-beads. The beads were washed and the translated protein was released by FLAG peptide (100μg/ml). Purified KPC1-FLAG-TEV-6xHIS and purified 6xHIS-KPC2 were added as indicated. Purified E1, UbcH5c, and ubiquitin, along with other necessary components were added as described under *Experimental Procedures*. A similar reaction was carried out with labeled p105 still present in the lysate in which it was translated (lanes 4-6). (ii) Attenuation of p105 ubiquitination by KPC2 is not attributed to a KPC2 deubiquitinating activity. In vitro translated and ^{35}S-labeled p105 was subjected to ubiquitination by KPC1-FLAG-TEV-6xHIS in a cell free system. The reactions were carried out in the absence or presence of KPC2 that was added along with (sim. – simultaneously) or following the addition of KPC1 (seq. – sequentially).

(B) Ubiquitination of in vitro translated and ^{35}S-labeled RING1B^{I53S} by 6xHIS-E6-AP in the presence or absence of 6xHIS-KPC2 was carried out in a reconstituted cell free system.

(C) Schematic representation of lysine residues in p105, p105K46-58R, p105Δ429-654, and p105Δ429-654;K29,46-58R. Numbers denote the respective residue along the protein sequence, and numbers next to K denote the respective lysine residue (numbered from 1 to 58) along the protein sequence.

(D) Cellular processing of FLAG-p105 species mutated in the ubiquitination sites along the C-terminal segment. cDNAs coding for WT and the indicated p105 mutants were transfected to HEK293 cells. Following SDS-PAGE of cell lysates, p105 and processed p50 were detected using anti-FLAG. Processing was assessed as described under Figure 2E.

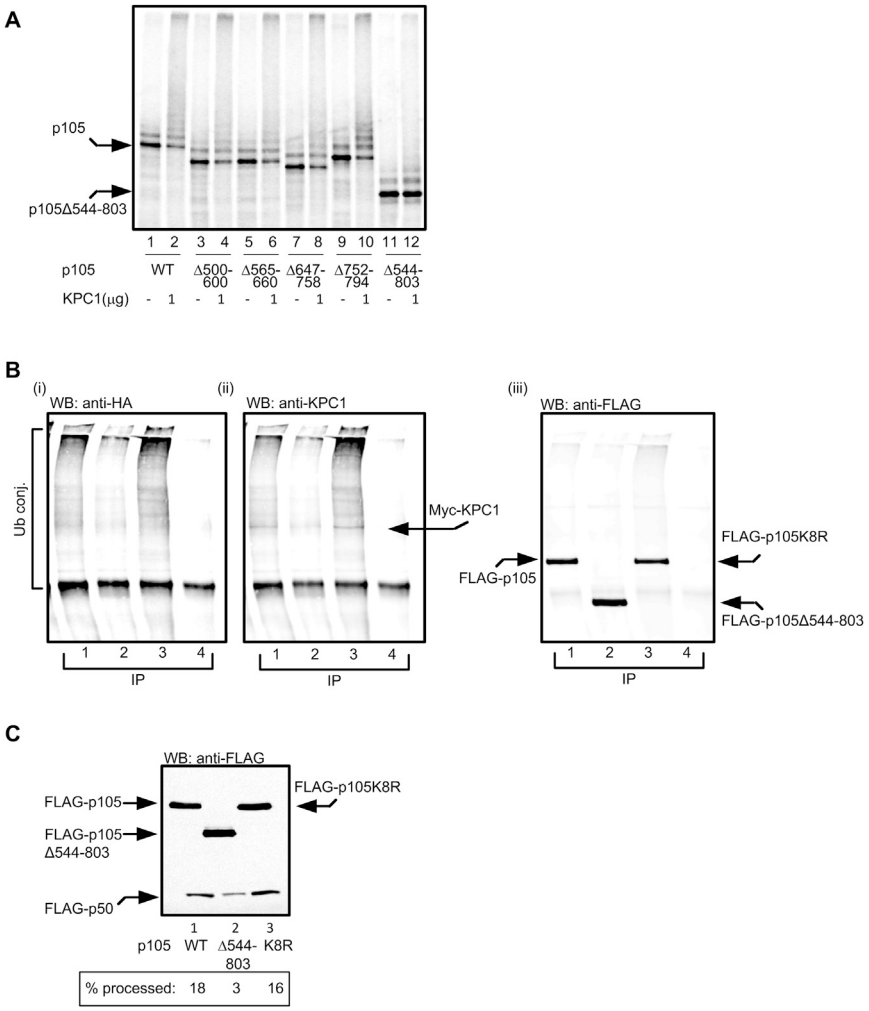

Figure S3. The p105 Ankyrin Repeats Are Essential for Its Ubiquitination and Processing, Related to Figure 3

(A) A single AR in p105 is dispensable for ubiquitination by KPC1 in a cell free system. The different deletion ^{35}S-labeled p105 species were ubiquitinated in a cell free reconstituted system in the presence or absence of KPC1-FLAG-TEV-6xHIS as indicated. The SDS-PAGE-resolved labeled proteins were visualized as described under *Experimental Procedures*.

(B) The internal lysines of the ARs are dispensable for ubiquitination of p105. HEK293 cells were transfected with cDNAs coding for FLAG-p105 (lane 1), FLAG-p105Δ544-803 (lane 2), or FLAG-p105K8R (lane 3; p105 in which all 8 lysines in the 6 ARs and in between them were substituted with arginines) along with Myc-KPC1 and HA-Ub (lanes 1-4). The different FLAG-p105 species were immunoprecipitated from cell lysates using immobilized anti-FLAG (IP; lanes 1-4), resolved via SDS-PAGE, and visualized using anti-HA (Bi), anti-KPC1 (Bii), or anti-FLAG (Biii).

(C) The internal lysines of the ARs are dispensable for processing of the molecule. HEK293 cells were transfected with cDNAs coding for FLAG-p105 (lane 1), FLAG-p105Δ544-803 (lane 2), or FLAG-p105K8R (lane 3). Proteins were resolved via SDS-PAGE, blotted onto nitrocellulose membrane, and p105 and p50 were detected using anti-FLAG. Processing was assessed as described under Figure 2E.

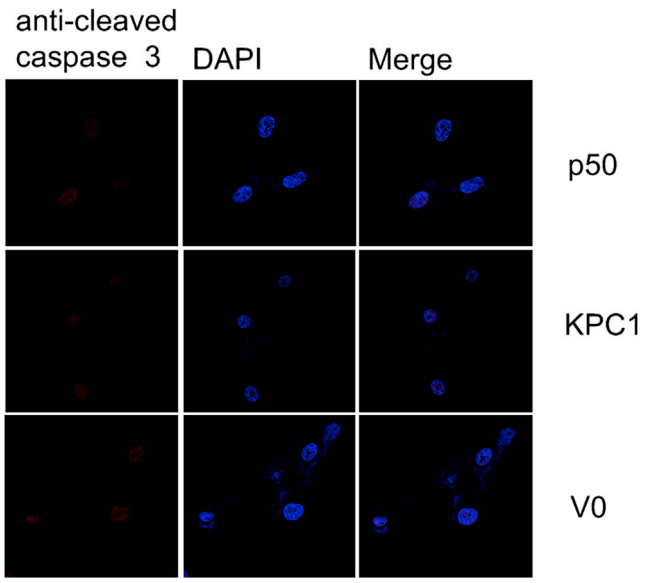

Figure S4. Effect of Overexpressed KPC1 and p50 on Cleaved Caspase 3 in Cultured Cells, Related to Figure 4
Anti-cleaved caspase 3 immunofluorescent staining of U87-MG cells stably overexpressing an empty vector (V0), Myc-KPC1, or FLAG-p50.

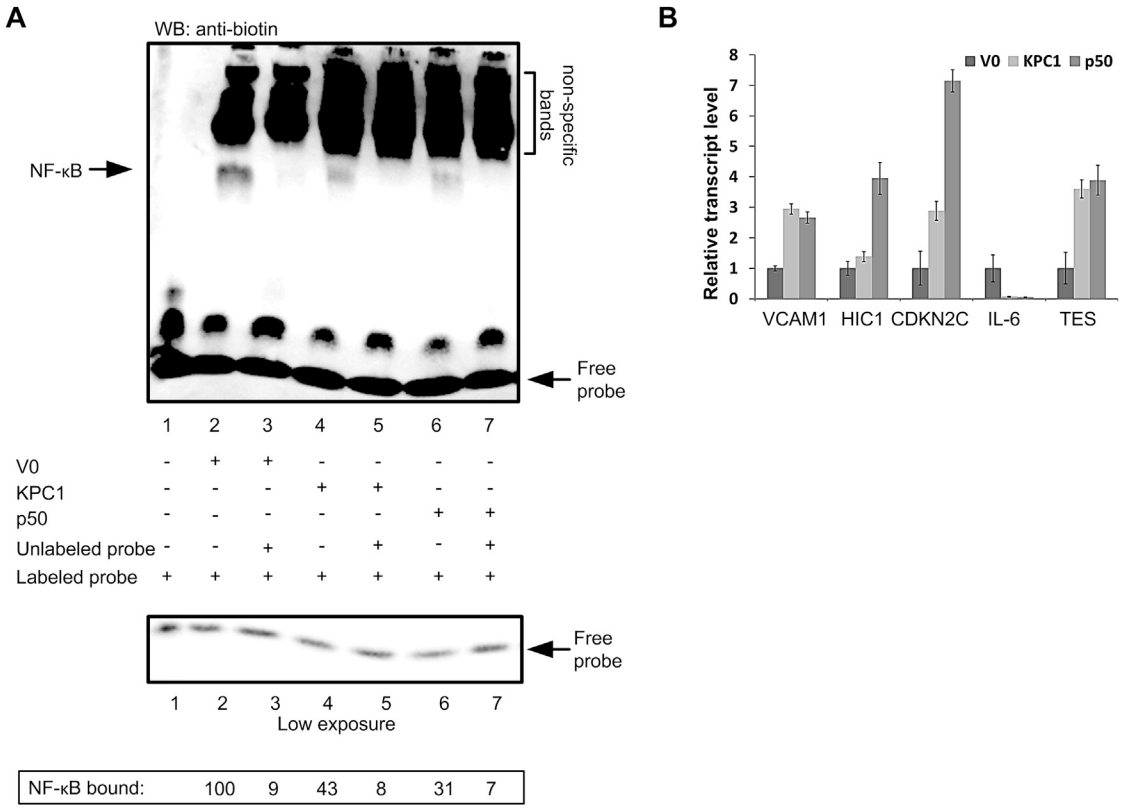

Figure S5. Analysis of U87-MG Xenografts Expressing V0, KPC1, or p50 for Binding of NF-κB to Its "Canonical" Binding Site and for Transcript Levels of Selected Human Genes, Related to Figures 5 and 6

(A) EMSA was carried out as described under *Experimental Procedures*. Values represent bound NF-κB where 100 is the value measured in an extract derived from cells expressing an empty vector (V0).

(B) Relative transcripts level of RNA isolated from U87-MG xenografts expressing V0, Myc-KPC1 or FLAG-p50. Expression of VCAM1, HIC1, CDKN2C, IL-6 and TES genes was analyzed using qRT-PCR as described under *Experimental Procedures*.

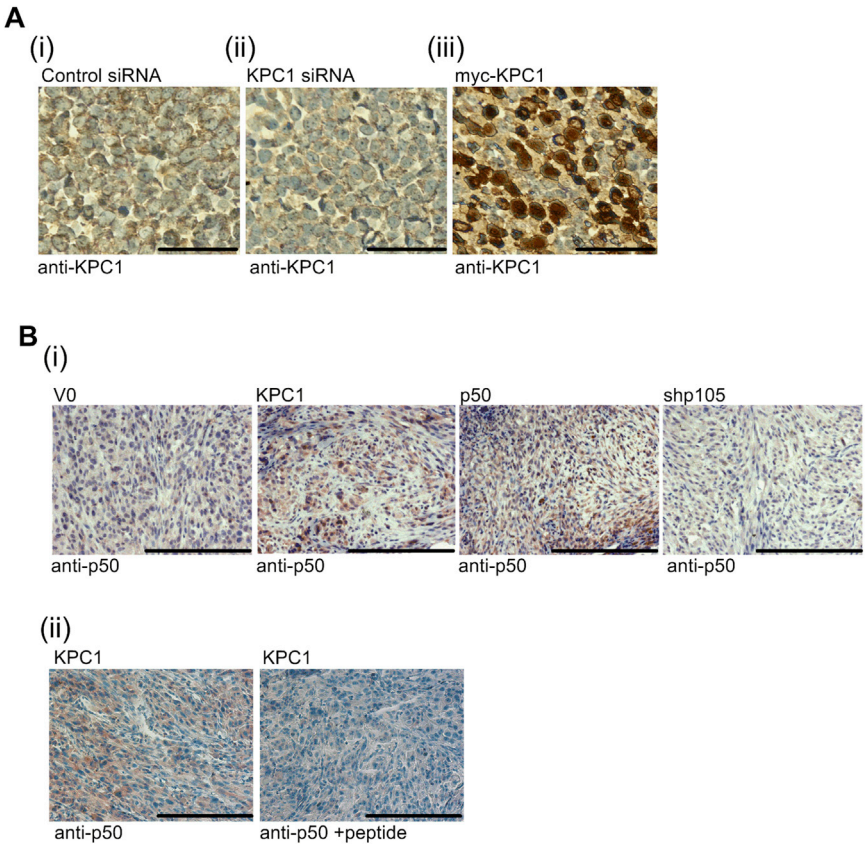

Figure S6. Validation of the Specificity of the Antibodies to KPC1 and p50 Used for Immunohistochemical Staining of Tumoral and Normal Human Tissues, Related to Figure 7

(A) Validation of the specificity of the anti-KPC1 antibody. Immunohistochemistry of KPC1 in HEK293 cells that were transfected with control siRNA (i), siRNA to silence KPC1 (ii) or with Myc-KPC1 (iii). All scale bars, 20 μm.

(B) Validation of the specificity of the anti-p50 antibody. (i) Immunohistochemistry of p50 in xenografts of U87-MG cells stably expressing V0, Myc-KPC1, FLAG-p50 or shRNA to p105. (ii) Immunohistochemistry of p50 in xenografts of U87-MG cells stably expressing Myc-KPC1 in the presence or absence of a specific blocking peptide (10 μg/ml) to the anti-p50 antibody. All scale bars, 100 μm.